STATISTICAL MODELING AND ANALYSIS OF HYBRID VLC/IRS-AIDED RF/THZ COMMUNICATION SYSTEMS

MS (RESEARCH) Thesis

By

KISHAN RAJESH TRIPATHI

DEPARTMENT OF ELECTRICAL ENGINEERING

INDIAN INSTITUTE OF TECHNOLOGY INDORE

JULY 2025

STATISTICAL MODELING AND ANALYSIS OF HYBRID VLC/IRS-AIDED RF/THZ COMMUNICATION SYSTEMS

A THESIS

Submitted in partial fulfillment of the
requirements for the award of the degree
of

MS (RESEARCH)

by

KISHAN RAJESH TRIPATHI

DEPARTMENT OF ELECTRICAL ENGINEERING
INDIAN INSTITUTE OF TECHNOLOGY INDORE

JULY 2025

INDIAN INSTITUTE OF TECHNOLOGY INDORE

CANDIDATE'S DECLARATION

I hereby certify that the work which is being presented in the thesis entitled **STATISTICAL MODELING AND ANALYSIS OF HYBRID VLC/IRS-AIDED RF/THZ COMMUNICATION SYSTEMS** in the partial fulfillment of the requirements for the award of the degree of **MS (RESEARCH)** and submitted in the **DEPARTMENT OF ELECTRICAL ENGINEERING**, Indian Institute of Technology Indore, is an authentic record of my own work carried out during the time period from **JULY 2023** to **JULY 2025** under the supervision of **Dr. Swaminathan Ramabadran, Associate Professor at Indian Institute of Technology Indore**.

The matter presented in this thesis has not been submitted by me for the award of any other degree of this or any other institute.

Kishan
08/06/2025

Signature of the student with date

(KISHAN RAJESH TRIPATHI)

. . . . . .

This is to certify that the above statement made by the candidate is correct to the best of my/our knowledge.

08/06/2025

Signature of the Supervisor of

MS (RESEARCH) thesis(with date)

(Dr. SWAMINATHAN RAMABADRAN)

. . . . . .

KISHAN RAJESH TRIPATHI has successfully given his/her **MS(R)** Oral Examination held on **07/07/2025**

(Swaminathan R)

Signature of the Supervisor of

MS (RESEARCH) thesis (with date)

Date: 07/07/2025

Saptarshi Ghosh

Convener, DPGC

Date: 07/07/2025

Acknowledgments

First and foremost, I would like to express my deepest gratitude to my supervisor, Dr. Swaminathan Ramabadran, for his exceptional guidance and unwavering support throughout the entire duration of my research. I am grateful for Dr. Ramabadran's patience and willingness to engage in thorough discussions, which greatly clarified my concepts and broadened my perspective as a researcher. His dedication and approach to research have continually inspired and motivated me to pursue excellence in my academic journey. I consider myself fortunate to have had the opportunity to work under his supervision.

I would also like to thank my colleagues in the lab Ms. Deepshikha Singh, Mr. Manoj Kokare, Mr. Nayim Ahmad, Mr. Prashant Sharma, Mr. Pranshu Singh, Ms. Vaishali Rohilla, and Mr. Vamshi Marri for the camaraderie and positive energy they brought to the lab each day.

I sincerely acknowledge IIT Indore and the Ministry of Education, Government of India, for supporting my MS (Research) by providing lab facilities and a TA scholarship, respectively.

I am deeply thankful to my parents for instilling in me the values of learning and the belief in the transformative power of education. I will forever remain indebted to them for their love and guidance.

Last but not least, I offer my heartfelt reverence to the lotus feet of Lord Krishna for His divine blessings.

Abstract

This thesis presents a comprehensive performance analysis of three hybrid communication systems designed to address the limitations of conventional indoor wireless technologies. The first system integrates a primary visible light communication (VLC) link with an intelligent reflecting surface (IRS)-aided radio frequency (RF) backup link. A hard-switching mechanism is employed, wherein data transmission persists over the VLC channel until the signal-to-noise ratio (SNR) drops below a threshold, triggering a switch to the IRS-assisted RF link. Analytical models are derived for key performance metrics including outage probability, outage capacity, and average bit error rate (BER), accounting for Lambertian radiation in VLC and Nakagami-*m* fading in RF. Monte Carlo simulations validate the theoretical expressions and demonstrate the robustness of the hybrid system over standalone VLC configurations.

The second part of this thesis investigates a hybrid VLC and terahertz (THz) communication system aimed at overcoming the limitations of standalone VLC in scenarios affected by non-line-of-sight (LoS) conditions and restricted coverage. The proposed system adopts a hard-switching strategy, whereby the THz link acts as a backup and is activated when the instantaneous SNR of the VLC link falls below a predefined threshold. The VLC link is modeled using Lambertian radiation characteristics, while the THz link is characterized using a generalized α-μ fading model, which captures small-scale multipath fading, molecular absorption, and pointing error-induced misalignments prevalent at THz frequencies. Analytical expressions are derived for key performance metrics, including outage probability and BER, and are further validated through Monte Carlo simulations. The results highlight the complementary strengths of VLC and THz channels, demonstrating that the hybrid system achieves improved reliability and spectral efficiency under diverse indoor propagation conditions.

The third part of this thesis proposes a novel hybrid communication architecture integrat-

ing VLC with an IRS-aided THz link. This system is designed to mitigate the severe path loss, blockage sensitivity, and alignment issues inherent in THz communication through IRS-based passive beamforming and dynamic reflection control. A hard-switching mechanism is employed where the IRS-assisted THz link supplements the VLC link under adverse channel conditions. The VLC channel is modeled via Lambertian emission, while the end-to-end THz channel gain is modeled as a cascaded product of generalized α-μ fading and stochastic pointing error distributions. The resultant channel statistics are expressed using multivariate Fox–H functions, enabling closed-form derivation of the outage probability and average BER. Numerical simulations validate the analytical expressions and demonstrate that the integration of IRS elements significantly enhances signal reliability and spatial coverage, even under challenging propagation conditions. This hybrid framework showcases the potential of intelligent surfaces in shaping future indoor wireless communication systems.

Contents

List of Figures

Chapter 1

Introduction

1.1 Background

The continuous surge in demand for wireless data services, driven by bandwidth-intensive applications and an increasing number of connected devices, necessitates exploring innovative solutions beyond traditional radio frequency (RF) technologies. Optical wireless communications, especially visible light communication (VLC), has emerged as a compelling alternative, primarily due to its abundant spectrum, high data rates, and inherent security advantages offered by line-of-sight (LoS) propagation [1, 2]. Despite these promising benefits, VLC systems are constrained by challenges such as susceptibility to blockage, ambient light interference, and limited non-line-of-sight (NLoS) capabilities, which restrict their reliability and coverage [3].

Integrating VLC with complementary technologies like RF, terahertz(THz), and intelligent reflecting surfaces (IRS) is recognized as a viable strategy to mitigate these limitations and enhance overall system performance [4, 5]. The RF band, although extensively utilized due to its widespread infrastructure and robustness, faces spectral congestion and interference issues in dense environments [6]. The THz band, on the other hand, offers significant bandwidth and potential for ultra-high data rates, though it suffers from severe path attenuation, antenna misalignment, and hardware imperfections [7, 8]. IRS technology has emerged as an innovative tool that can dynamically control the propagation environment, significantly improving signal strength, reliability, and coverage by intelligently reflecting electromagnetic waves [9, 10].

Hybrid optical–wireless communication systems, particularly VLC combined with RF,

IRS, and THz technologies, present a novel approach capable of leveraging each technology's strengths. This thesis investigates the integration and performance analysis of hybrid VLC/IRS-aided RF, hybrid VLC/THz, and hybrid VLC/IRS-aided THz communication systems, aiming to comprehensively understand their potentials and address existing limitations through theoretical modeling, analytical techniques, and simulation validations.

1.2 Literature Review

Hybrid optical–wireless communication systems have received considerable research attention due to the complementary strengths of VLC, RF, IRS, and THz technologies. VLC systems, which operate in the optical spectrum, offer advantages such as unlicensed bandwidth, low electromagnetic interference, and inherent security stemming from their LoS requirement [1, 2]. However, their susceptibility to shadowing and obstruction severely limits their reliability and widespread applicability [3].

To address these limitations, several studies have investigated diverse mitigation strategies. For instance, the work in [11] examines jamming resilience in VLC systems using CRC-16 codes and reports improvements in robustness against intentional interference. In the context of outdoor VLC links, [12] explores the use of laser-based optical transmitters with narrow divergence angles, enhancing communication range and stability. Addressing the nonlinearity of light emitting diodes (LEDs), which adversely affects signal fidelity at high data rates, [13] introduces a nonlinear equalization method based on the Volterra series, demonstrating its effectiveness in high-speed wavelength division multiplexing (WDM) VLC systems.

In addition to transmitter-side improvements, receiver-side enhancements have also been studied. In [14], the authors show that NLoS reflections can be leveraged to increase optical gain and enable mobile connectivity, especially in scenarios where LoS is intermittently blocked. This finding challenges the conventional assumption that NLoS components degrade performance and instead positions them as an auxiliary propagation path in dynamic environments. Furthermore, hybrid link strategies have been proposed to combine VLC with RF communication. The study in [15] demonstrates a practical handover mechanism using dual receivers, enabling seamless transition between VLC and RF links to maintain service continuity during mobility or link degradation.

Collectively, these contributions highlight the active research community's efforts to overcome the practical limitations of VLC through signal processing, hardware enhancements, and system-level hybridization. However, many of these approaches are constrained by assumptions of ideal conditions or limited scalability, suggesting a need for more adaptable and robust hybrid models that can maintain performance under diverse environmental and channel conditions.

To address the limitations inherent in VLC systems, particularly their sensitivity to obstruction and dependence on LoS propagation, recent research has focused on the integration of IRS with RF communication technologies as a promising enhancement strategy [9, 10]. IRS technology offers the capability to reconfigure the wireless propagation environment dynamically by intelligently adjusting the phase of incident signals, thereby enhancing signal strength, improving spectral efficiency, and expanding coverage without the need for additional RF power or infrastructure [16]. For example, [16] presents a detailed performance analysis of IRS-aided RF systems over Rayleigh fading channels and reports considerable improvements in reliability and outage probability relative to conventional RF links. These findings have motivated the incorporation of IRS into hybrid VLC/RF frameworks, where IRS can compensate for the limitations of the VLC component. In such configurations, IRS assists in maintaining robust communication under fluctuating indoor conditions, effectively mitigating signal blockage and enhancing link resilience [6, 17].

In parallel, THz communication has been widely investigated as a viable candidate for supporting the ultra-high data rate demands of future wireless systems, particularly beyond 5G and into the 6G era. Despite its vast spectral availability and theoretical support for multi-gigabit transmissions, THz communication faces critical practical challenges. These include severe molecular absorption-induced attenuation, difficulties in achieving precise antenna alignment due to the highly directional nature of THz signals, and various hardware-induced impairments [7, 18, 19]. To accurately characterize the propagation behavior in the THz band, a range of channel modeling techniques have been proposed. Early efforts, such as the path-loss-based models introduced in [20], provided a foundational understanding of frequency-dependent attenuation in the 275–400 GHz range. More complex representations, including multi-ray propagation models developed in [21], account for environmental reflections and scattering effects, providing a more realistic depiction of THz signal behavior in indoor and structured environments.

A seminal contribution by Jornet and Akyildiz [22] introduced an electromagnetic channel model that incorporated the impact of molecular absorption, laying the groundwork for subsequent studies. These models were further refined to accommodate various deployment scenarios, including nano-scale communication systems [23, 24], intra-body communication networks [25], and general indoor wireless settings [26, 27]. However, many of these earlier works omitted the effect of small-scale fading, which becomes non-negligible in practical THz deployments due to scattering from particles, objects, and surfaces. Recognizing this, more recent studies have integrated stochastic fading models such as Rayleigh, Rician, and Nakagami-m distributions to capture the multipath dynamics of THz channels under realistic propagation conditions [28, 29, 30, 31]. These models provide a more accurate framework for performance analysis and system design, especially for applications involving mobility, indoor environments, or biological mediums where fading and misalignment are prominent.

A considerable body of research has also been devoted to addressing antenna misalignment issues that arise in THz communication systems, particularly due to the use of highly directive antennas with narrow beamwidths [29, 32]. While such antennas are essential for minimizing path loss and achieving high directivity gains, they introduce a significant vulnerability to alignment errors, especially in dynamic or unstable deployment environments. Existing literature has primarily adopted deterministic modeling approaches to characterize the impact of beam misalignment. For example, [29] and [32] analyze the influence of mechanical deviations on beam alignment but do not fully capture the stochastic nature of real-world perturbations such as thermal expansion, wind-induced sway, or micro-vibrations in high-rise buildings. The limitations of these deterministic models have been noted in studies such as [33], which emphasize the need for statistical frameworks capable of accounting for random alignment deviations over time.

To address these shortcomings, this thesis explores the integration of IRS into THz systems as a mechanism to dynamically compensate for misalignment and associated fading effects. The adaptive beam steering and passive reconfiguration capabilities of IRS technology provide a promising solution to maintain effective link quality despite physical misalignments or channel instability, thus enhancing the overall reliability and robustness of THz communication systems.

In addition to alignment challenges, hardware impairments present a significant barrier to the practical deployment of THz systems. Phase noise, power amplifier non-linearities,

and in-phase/quadrature (I/Q) imbalances are among the most impactful distortions encountered in THz transceiver design. These impairments degrade signal integrity, reduce achievable throughput, and complicate receiver design. Analytical studies and experimental validations have highlighted the severity of these issues in realistic operating conditions [34, 35, 36, 37]. For instance, [34] and [35] provide empirical evidence of performance degradation caused by phase noise and I/Q imbalance in high-frequency direct-conversion systems.

Despite their drawbacks, direct-conversion (zero-IF) transceiver architectures are often preferred in THz system design due to their relatively low complexity, cost efficiency, and suitability for integration into compact hardware platforms [38, 39]. As such, there is growing emphasis on developing compensation techniques and robust circuit designs that can mitigate these impairments without significantly increasing system complexity or power consumption. This ongoing research underscores the critical need to jointly consider hardware non-idealities and channel effects in system-level analyses of THz communication networks.

The convergence of visible light communication (VLC), radio frequency (RF), terahertz (THz), and intelligent reflecting surface (IRS) technologies into unified hybrid communication frameworks has emerged as a promising research direction. These hybrid communication systems are designed to harness the complementary strengths of the constituent technologies—namely, the high-capacity line-of-sight links offered by VLC, the robustness and penetration capability of RF, the ultra-wide bandwidth of THz communications, and the reconfigurability of IRS—to enable the development of more resilient and high-performance wireless networks. Numerous studies on hybrid VLC/RF systems have demonstrated their potential in significantly improving link reliability and performance metrics, particularly outage probability and bit error rate (BER). These improvements are often achieved through adaptive link selection mechanisms that respond dynamically to variations in channel quality, ensuring that the most suitable communication mode is utilized at any given moment [17].

Similarly, hybrid VLC/THz architectures have gained traction for their ability to support ultra-high data rate transmissions while maintaining reliable connectivity. These systems exploit VLC's secure and high-throughput characteristics in short-range indoor environments, while simultaneously utilizing the expansive bandwidth offered by the THz spectrum for backhaul or high-density user scenarios. The inclusion of IRS in such configurations further

enhances system adaptability by reconfiguring the propagation environment, enabling efficient signal redirection and overcoming obstacles that would otherwise disrupt LoS paths.

While substantial progress has been made in characterizing the performance of individual and dual-technology hybrid systems, the integration of all four technologies—particularly hybrid VLC/IRS-aided THz systems—remains insufficiently explored. In particular, there is a notable lack of comprehensive analytical models that capture the interplay of VLC and THz propagation characteristics, IRS-induced channel modifications, and system-level performance under practical deployment constraints. Existing works often rely on simplified assumptions or partial system models, limiting their applicability to real-world scenarios.

This thesis addresses these critical gaps by formulating rigorous analytical frameworks for hybrid VLC/IRS-aided THz systems. It includes the derivation of closed-form expressions for key performance metrics, supported by extensive Monte Carlo simulations to validate theoretical findings under a range of channel and hardware conditions. Moreover, the thesis explores adaptive switching and combining schemes tailored to hybrid environments, contributing a holistic performance evaluation of these emerging systems. Through these efforts, the research aims to advance the state-of-the-art in hybrid optical–wireless communications and provide foundational insights for the development of robust, high-capacity indoor communication networks of the future.

1.3 Motivations and Contributions

1.3.1 Chapter 2

The motivations behind the work in Chapter 2 are summarized as follows:

- The integration of IRS with RF communication systems represents a progressive leap in wireless technology, offering promising improvements in signal strength, bandwidth efficiency, and network coverage. These systems have been the focus of extensive research and development, yielding significant advancements in RF communications. However, the exploration of usage of IRS to enhance VLC systems, especially in hybrid configurations that also incorporate RF technology, is still in its nascent stages.

- This notable research gap is driven by the unique challenges and opportunities pre-

sented by VLC technologies. VLC systems are known for their high bandwidth, low latency, and the inherent security of light-based transmission, making them highly attractive for indoor communication scenarios such as smart homes, offices, and industrial environments. However, VLC's reliance on LoS operations and its susceptibility to ambient light interference and physical obstructions can significantly limit its reliability and effectiveness. As mentioned before, prior works [1, 6, 40, 41, 3, 4, 5, 9, 10, 16, 6, 11, 12, 14] either do not explore or only minimally address comprehensive statistical performance.

- To the best of our knowledge, there is currently no existing literature that explores the comprehensive performance analysis of IRS-aided hybrid RF/VLC system, over Lambertian radiation emission and Nakagami-*m* fading channel, in terms of outage probability, outage capacity, and average BER.

- This motivated us to address the existing research gap.

The contributions of the work in Chapter 2 are summarized as follows:

- We introduce an advanced IRS-aided hybrid RF/VLC system specifically designed for indoor environments. This system innovatively integrates VLC and RF communication technologies, employing hard-switching scheme based on the instantaneous SNR. This approach ensures optimal signal quality and reliability by leveraging the most suitable communication medium in real-time, depending on environmental conditions and system performance.

- We have developed comprehensive analytical models for the hybrid system by statistically deriving the closed-form expressions for the probability density function (PDF) and cumulative distribution function (CDF) of instantaneous SNR of both the RF and VLC channels. Initially, the PDF and CDF of the instantaneous SNR of the RF channel are derived under Nakagami-*m* fading conditions, capturing the multipath fading characteristics specific to RF communication. Subsequently, the PDF and CDF of the instantaneous SNR of the VLC channel are obtained considering the Lambertian radiation emission pattern, which models the intensity distribution of the VLC source.

- Building upon these foundational PDF and CDF expressions, we have proceeded to calculate critical performance metrics for the hybrid VLC/IRS-aided RF system. This

includes deriving the outage probability, which quantifies the likelihood of the system operating below a specified SNR threshold, and the outage capacity, representing the maximum achievable rate under outage constraints. Furthermore, we evaluated the average BER of the hybrid system, providing insights into its error performance.

- Our theoretical findings are rigorously validated through extensive Monte-Carlo simulations, which confirm the accuracy and reliability of our derived analytical expressions. This validation process demonstrates the practical applicability of our theoretical insights and ensures that our proposed system design can achieve the expected performance improvements in real-world scenarios.

- We conduct an in-depth parameter study to assess the impact of various system variables on the performance of the hybrid communication system. This study includes analyses of how changes in IRS configuration and other system parameters affect key performance metrics. The outcomes of this analysis provide valuable insights for system tuning and highlight the robustness of our proposed solution across different configurations and conditions.

These contributions not only demonstrate the feasibility of the proposed IRS-aided hybrid RF/VLC system but also highlight its potential to significantly enhance the efficiency and reliability of indoor wireless communications. The insights gained from this research could serve as a cornerstone for future developments in hybrid communication technologies.

1.3.2 Chapter 3

The motivations behind the work in Chapter 3 are summarized as follows:

- VLC systems, despite their high bandwidth and inherent security, suffer from key limitations in real-world environments, especially due to their dependency on line-of-sight (LoS) conditions and high sensitivity to obstructions. These limitations result in reliability issues, particularly in dynamic or non-line-of-sight indoor scenarios.

- Terahertz (THz) communication has recently emerged as a compelling high-frequency wireless alternative capable of providing ultra-high data rates due to the availability of large bandwidth. However, THz systems also suffer from high path loss and signal

degradation due to molecular absorption and atmospheric attenuation, especially over longer ranges or under misalignment.

- Although existing research has addressed standalone VLC or THz systems, very limited literature exists on their joint use in hybrid communication architectures. In particular, the design and performance analysis of a hybrid VLC/THz communication system using analytical models remains under-explored. There is a strong need to model such hybrid systems under realistic channel assumptions like Lambertian radiation for VLC and α-μ fading for THz.

- There is also a lack of performance analysis study for such hybrid systems, especially in terms of key metrics such as outage probability, BER, and outage capacity. This gap motivates the development of rigorous mathematical frameworks for the analysis of such systems.

The contributions of the work in Chapter 3 are summarized as follows:

- We propose a hybrid VLC/THz communication system that uses a hard-switching mechanism to select between VLC and THz links based on the instantaneous SNR, ensuring reliability in challenging propagation environments.

- We model the VLC channel using Lambertian emission patterns and the THz channel using the generalized α-μ fading distribution, thereby capturing both small-scale fading and environmental attenuation effects.

- We derive closed-form expressions for outage probability, average BER, and outage capacity. These expressions provide theoretical insight into the system's performance under different conditions.

- The BER for the THz link is derived using Gauss–Laguerre quadrature to overcome the complexity of the α-μ fading-based CDF.

- All analytical results are validated using Monte-Carlo simulations, confirming the accuracy of our models.

- We further present a detailed parametric study to examine the impact of THz link parameters such as the fading severity and path-loss factors on the overall hybrid system performance.

This chapter establishes the potential of VLC/THz hybrid systems to serve as reliable high-data-rate indoor wireless communication solutions, and lays a solid foundation for next-generation wireless system design involving optical and THz technologies.

1.3.3 Chapter 4

The motivations behind the work in Chapter 4 are summarized as follows:

- While the hybrid VLC/THz system introduced in Chapter 3 shows improved performance over standalone VLC, it still suffers from limitations due to the inherent vulnerability of THz links to path loss, molecular absorption, and misalignment.

- IRS offer an effective solution for overcoming these challenges in THz links by enabling dynamic control over the wireless environment. However, the performance of IRS-assisted THz systems in hybrid VLC scenarios has not been extensively studied, particularly using advanced statistical models that incorporate generalized fading and pointing errors.

- Additionally, there is a lack of tractable models for the distribution of the IRS-aided THz channel gain, which is crucial for accurate performance analysis. The need to account for IRS gain, path loss, and fading in a unified manner motivates the development of new analytical frameworks using Fox's H-function.

The contributions of the work in Chapter 4 are summarized as follows:

- We propose a novel hybrid VLC/IRS-aided THz system, where the IRS-aided THz link acts as a backup to the primary VLC link under a hard-switching decision rule based on the instantaneous SNR threshold.

- The THz channel is modeled as a cascaded channel incorporating generalized α-μ fading, stochastic pointing errors, and deterministic path loss due to molecular absorption. The complete channel gain is expressed using tractable Fox's H-function.

- We derive closed-form analytical expressions for the outage probability and average BER. The BER expression for the THz link is computed using the Gauss–Laguerre quadrature method due to the analytical intractability of the exact integral.

- Monte-Carlo simulations validate the theoretical derivations, demonstrating their applicability in realistic scenarios.

- The performance results confirm that the IRS-aided hybrid VLC/THz system significantly outperforms both standalone VLC and traditional hybrid VLC/THz systems, especially in low-SNR regimes. The system shows improved reliability and BER performance due to the IRS elements.

- A detailed analysis is also conducted to assess the effect of the number of IRS elements and fading parameters on system performance, revealing the benefits of scalable IRS deployment in improving THz reliability.

This chapter confirms the promise of IRS-enhanced THz communications in optical–wireless hybrid systems and opens the path to intelligent, high-frequency indoor networking architectures suitable for 6G and beyond.

1.4 Organization of the Thesis

The remainder of this thesis is organized as follows:

- **Chapter 2** introduces an IRS-aided hybrid RF/VLC communication system for indoor wireless environments. It presents the system model, statistical channel characterization using Lambertian radiation and Nakagami-m fading, and derives analytical expressions for outage probability, average BER, and outage capacity. Monte-Carlo simulations are performed to validate the analytical findings.

- **Chapter 3** proposes a hybrid VLC/THz communication system to address the limitations of standalone VLC links. The VLC and THz channels are modeled using Lambertian emission and α-μ fading, respectively. Closed-form expressions for outage probability, average BER, and outage capacity are derived and validated using simulation.

- **Chapter 4** presents a hybrid VLC/IRS-aided THz system, where the backup THz link is enhanced using intelligent reflecting surfaces. The cascaded THz channel gain is modeled using Fox–H functions to incorporate generalized fading and pointing errors.

Analytical expressions for outage probability and BER are derived and validated with Monte-Carlo simulations.

- **Chapter 5** summarizes the key insights and contributions across all chapters. It provides a unified comparison of the proposed hybrid systems and offers perspectives for extending this work to multi-user, multi-hop, and real-time adaptive scenarios in future research.

Chapter 2

Hybrid VLC/IRS-Aided RF Communication Systems

2.1 Introduction

Hybrid VLC/IRS-Enhanced RF communication provides notable advantages such as improved reliability, enhanced signal quality, and efficient spectrum utilization, especially in indoor environments. However, standalone VLC links suffer from limitations like LoS dependency, shadowing, and sensitivity to alignment and ambient light conditions. In this chapter, we introduce a hybrid VLC/RF communication system integrated with an IRS, designed to overcome these limitations and ensure robust connectivity. The proposed model employs a VLC-based primary transmission link and an IRS-assisted RF link as a backup, with a hard-switching mechanism based on a predefined SNR threshold. The system continues transmission via the VLC link until the SNR drops below the threshold, upon which it seamlessly switches to the RF link. The VLC channel is modeled using the Lambertian emission profile, while the RF channel is characterized using Nakagami-m fading. The main objective of this work is to evaluate the system-level performance of the proposed architecture by deriving closed-form expressions for key performance metrics such as outage probability, outage capacity, and average BER. The analytical results are corroborated with extensive Monte-Carlo simulations, demonstrating the performance improvement achieved through IRS-assisted RF integration over standalone VLC systems.

2.2 Organisation of Chapter

The remaining sections of this chapter are structured as follows: Section 2.3 introduces the system and channel models for the hybrid VLC/IRS-enhanced RF communication system, including the derivation of the PDF and CDF for both VLC and IRS-assisted RF links. In Section 2.4, a detailed analytical performance evaluation is carried out, focusing on outage probability, outage capacity, and BER. Section 2.5 presents numerical results alongside Monte-Carlo simulations, offering insights into the influence of various system parameters. Finally, Section 2.6 concludes the chapter by summarizing the key findings and suggesting directions for future work in hybrid communication systems.

2.3 System Model

This chapter introduces an innovative IRS-aided hybrid RF/VLC communication system as shown in Fig. 2.1, meticulously crafted to enhance indoor wireless communication environments. The core concept lies in the utilization of an IRS-aided RF system alongside a primary VLC link. The system is designed to switch from the VLC to the RF link based on a predefined threshold value. This switching is triggered when the SNR of the VLC link falls below the threshold value, thereby ensuring the system can maintain reliable communication by transitioning to the IRS-assisted RF backup link. This strategy enhances the robustness and efficiency of the system by effectively managing transitions between different communication technologies under varying channel conditions.

2.3.1 VLC Channel Model

In the assumed indoor VLC scenario, LED transmitter mounted overhead is considered as the primary light source and communication transmitter, ensuring a LoS communication path to the user equipment positioned below, as depicted in Fig. 2.2.

The VLC system's channel gain h_k is given by [42]

$$h_k = \frac{(m+1)A_p R_p}{2\pi r_k^2} \cos^m(\phi_k) T(\psi_k) g(\psi_k) \cos(\psi_k), \tag{2.1}$$

where A_p is the active area of the photodiode, R_p denotes the photodiode's responsivity, $T(\psi_k)$ and $g(\psi_k)$ represent the gains from the optical filter and concentrator, respectively, m

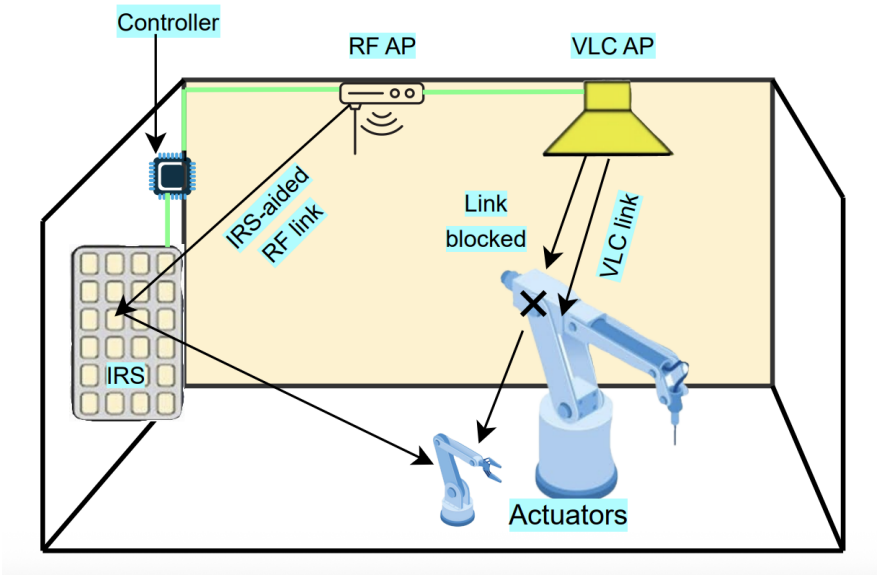

Figure 2.1: Hybrid VLC/IRS-aided RF system model.

is the Lambertian order of emission determined by the semi-angle at the half luminance ϕ_k, and r_k denotes the horizontal link distance from the center of the illuminated area to the k^{th} actuator.

The optical concentrator's gain, $g(\psi_k)$, is defined as

$$g(\psi_k) = \frac{n^2}{\sin^2(\psi_{\text{FOV}})}, \tag{2.2}$$

where n is the refractive index and ψ_{FOV} is the actuator's field of view.

The channel gain h_k can be expressed as

$$h_k = \chi \left(r_k^2 + L^2\right)^{-\frac{m+3}{2}}, \tag{2.3}$$

where $m = -\frac{1}{\log_2 \cos(\phi_k)}$ and χ encapsulates the impacting parameters and is written as

$$\chi = \frac{(m+1)L^{m+1}T(\psi_k)G(\psi_k)R_p A_p}{2\pi}. \tag{2.4}$$

Given r_k is uniformly distributed across the illuminated area, the pdf of r_k can be written as

$$f_{r_k}(r_k) = \frac{2r_{\max}}{r_k^2}, \tag{2.5}$$

where r_{max} is the maximum cell radius shown in the Fig. 2.2.

The instantaneous SNR γ_v of VLC link is given as

$$\gamma_v = \overline{\gamma}_v h_k^2 \tag{2.6}$$

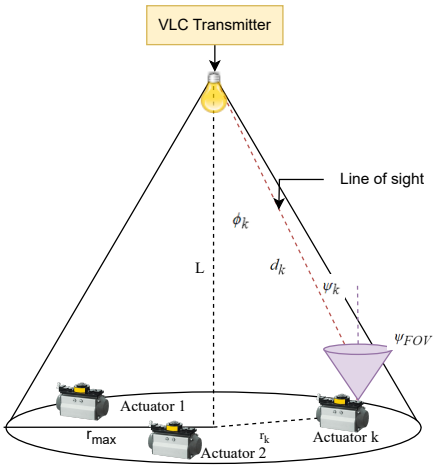

Figure 2.2: VLC system model.

where $\overline{\gamma}_v = \frac{\rho P^2}{N_0 B}$, ρ is the electrical-to-optical conversion ratio, P is the transmitted optical power, N_0 is the noise spectral density, and B is the baseband modulation bandwidth. Now, we derive the PDF of h_k^2 by transforming the variable r_k in terms of h_k by using (2.3) and (2.5) . The PDF of h_k^2 directly leads to the PDF of the instantaneous SNR γ_v, which is given by

$$f_{\gamma_v}(\gamma_v) = \frac{\left(\chi L^{m+1}\right)^{\frac{2}{m+3}} \left(\overline{\gamma}_v\right)^{\frac{1}{m+3}} \gamma_v^{-\frac{1}{m+3}-1}}{r_{\max}^2 (m+3)} \tag{2.7}$$

To derive the CDF of the VLC channel in terms of instantaneous SNR γ_v, we have integrated the PDF of instantaneous SNR, which is given by (2.7), over its operational range. Now, the CDF is computed as

$$F_{\gamma_v}(\gamma_v) = \int_{\gamma_{\min}}^{\gamma_{\max}} f_{\gamma_v}(\gamma_v)\, d\gamma_v, \tag{2.8}$$

where $\gamma_{\min}$ and $\gamma_{\max}$ are the lower and upper bounds of the SNR [43], respectively.

After solving (2.8), the CDF is expressed as

$$F_{\gamma_v}(\gamma_v) = \mathscr{B} - \Upsilon \gamma_v^{-\frac{1}{m+3}}, \tag{2.9}$$

where $\mathscr{B} = \frac{r_{max}^2 + L^2}{r_{max}^2}$ and $\Upsilon = \frac{\left(\chi^2 \overline{\gamma}_v\right)^{\frac{1}{m+3}}}{r_{max}^2}$ are constants.

2.3.2 IRS-Assisted RF Channel Model

As depicted in Fig. 2.3, our system model involves an IRS-aided RF communication, where a single-antenna RF access point communicates with a destination actuator, facilitated by IRS equipped with N reflecting elements.

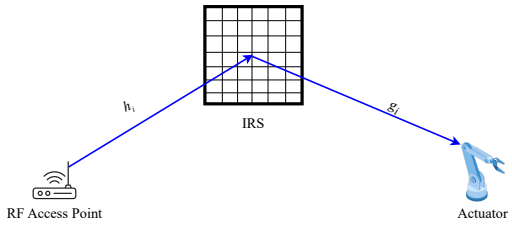

Figure 2.3: IRS-aided RF system model.

The channel coefficients for the RF access point to IRS (h_i) and from IRS to the actuator (g_i) are expressed as [16]

$$h_i = \alpha_i e^{j\theta_i}, \quad g_i = \beta_i e^{j\psi_i}, \tag{2.10}$$

where α_i and β_i represent the amplitude gains, while θ_i and ψ_i denote the phase shifts of the RF signals on the respective links. The channel gains h_i and g_i are modeled using Nakagami-m fading model [44]. We have taken this fading model because this gives us flexibility to switch to various other fading models. For instance, if we keep the Nakagami-m fading severity parameter $m_{rf} = 1$, the fading channel model resembles the Rayleigh fading model and when $m_{rf} > 5$, the fading channel model approximately resembles Rician fading model. Hence, just by varying the fading severity parameter, we get the leverage to analyze the performance of the system over multiple fading channel models intuitively.

Optimal phase adjustments at the IRS (ϕ_i) are calculated to ensure constructive interference of the reflected signals at the actuator leading to the maximized end-to-end SNR, which is given by

$$\gamma_r = \frac{\left(\sum_{i=1}^{N} \alpha_i \beta_i\right)^2 E_s}{N_0} = \frac{A^2 E_s}{N_0}, \tag{2.11}$$

where A is defined as the effective amplitude gain from all IRS elements, with E_s representing the transmitted signal energy and N_0 denoting the noise power spectral density. Under the assumption that A follows Nakagami-m fading, A^2 is modeled as a gamma-distributed random variable, based on which the PDF and CDF of the instantaneous SNR are derived

through the transformation of random variables and the PDF and CDF of the instantaneous SNR are, respectively, given by

$$f_{\gamma_r}(\gamma_r) \approx \frac{\left(\frac{\gamma_r}{\overline{\gamma}_r}\right)^{\frac{a-1}{2}} \exp\left(-\frac{\sqrt{\gamma_r}}{\sqrt{\overline{\gamma}_r b^2}}\right)}{2\Gamma(a) b^a \sqrt{\frac{\overline{\gamma}_r}{\gamma_r}}} \tag{2.12}$$

$$F_{\gamma_r}(\gamma_r) \approx \frac{\gamma\left(a, \sqrt{\frac{\gamma_r}{b^2 \overline{\gamma}_r}}\right)}{\Gamma(a)} \tag{2.13}$$

where $\overline{\gamma}_r$ is the average SNR of RF link, a and b are the shape and scale parameters derived from the distribution of the cascaded fading channels and these parameters are dependent on the fading severity parameter m_{rf} and the shape parameter Ω_{rf} of individual Nakagami-m channel, and $\gamma(\cdot,\cdot)$ is the lower incomplete gamma function [45].

2.4 Performance Analysis

This section presents the performance analysis of IRS-aided hybrid RF/VLC system. The expressions for the outage probability, outage capacity and average BER are derived for the proposed system considering hard-switching scheme.

2.4.1 Outage Probability

Outage probability is a critical performance metric in communication systems, indicating the likelihood that the system's SNR falls below a specified threshold, thereby compromising the link's reliability. In the hybrid model we have presented, the system employs a predefined SNR threshold for switching between communication links. The primary VLC link, operating under LoS conditions with Lambertian emission serves as the default transmission path. If the instantaneous SNR of the VLC system drops below the threshold SNR, γ_{th}, the system dynamically switches to the IRS-assisted RF backup link. This ensures continuous communication by leveraging the RF link when VLC performance degrades. The outage probability for the hybrid system is thus determined by the probability that both the VLC and the IRS-assisted RF link SNRs fall below γ_{th}, indicating a system outage. Thus, the outage probability is expressed as is expressed as

$$P_{\text{out}} = F_{\gamma_v}(\gamma_{th}) F_{\gamma_r}(\gamma_{th}), \tag{2.14}$$

where $F_{\gamma_v}(.)$ and $F_{\gamma_r}(.)$ are the CDFs of the instantaneous SNR of the VLC and RF systems, which are given by (2.9) and (2.13), respectively. These functions are evaluated at the outage threshold γ_{th}. Hence, the final analytical expression for the outage probability of the hybrid system is written as

$$P_{\text{out}} = \left(\mathscr{B} - \Upsilon(\gamma_{th})^{-\frac{1}{m+3}}\right) \frac{\gamma\left(a, \sqrt{\frac{\gamma_{th}}{b^2\bar{\gamma}_r}}\right)}{\Gamma(a)} \tag{2.15}$$

2.4.2 Outage Capacity

Outage capacity measures the probability that the normalized capacity of the communication system falls below a predefined threshold, denoted as C_{th}. The normalized capacity for a given instantaneous SNR γ is expressed as [46]

$$C_{\text{norm}} = \log_2(1+\gamma) \tag{2.16}$$

Now, the outage capacity of the hybrid system is given by

$$\begin{aligned} C_{\text{out}} &= \Pr\left(\log_2(1+\gamma_v) \leq C_{\text{th}} \cap \log_2(1+\gamma_r) \leq C_{\text{th}}\right) \\ &= \Pr\left(\gamma_v \leq 2^{C_{\text{th}}} - 1 \cap \gamma_r \leq 2^{C_{\text{th}}} - 1\right) \\ &= F_{\gamma_v}(2^{C_{\text{th}}} - 1) F_{\gamma_r}(2^{C_{\text{th}}} - 1) \end{aligned} \tag{2.17}$$

From (2.17), and using (2.9) and (2.13), the final analytical expression for the outage capacity of the hybrid system is given by

$$C_{\text{out}} = \left(\mathscr{B} - \Upsilon(2^{C_{\text{th}}} - 1)^{-\frac{1}{m+3}}\right) \frac{\gamma\left(a, \sqrt{\frac{2^{C_{\text{th}}}-1}{b^2\bar{\gamma}_r}}\right)}{\Gamma(a)} \tag{2.18}$$

2.4.3 Average BER

We assume sub-carrier intensity-modulation-based $M-$ary phase-shift keying (MPSK) technique for VLC and MPSK scheme for RF communication. The generalized governing symbol error rate (SER) expression for MPSK modulation scheme for a given instantaneous SNR γ has been utilized to calculate the average SER using the CDF-based approach and is given by

$$P_{\text{ser}} = \frac{t\sqrt{u}}{2\sqrt{2\pi}} \int_0^{\infty} \frac{F_{\gamma}(\gamma)}{\sqrt{\gamma}} e^{-\frac{u\gamma}{2}} d\gamma, \tag{2.19}$$

where $F_{\gamma}(\gamma)$ indicates the CDF of either VLC or RF link, t and u indicate modulation specific parameters as shown in Table II. These parameters can be varied to obtain the average SER of the required MPSK signalling scheme.

Table 2.1: Values of t and u for Different Modulation Schemes

t	u	**Modulation Scheme**
1	2	BPSK
2	1	QPSK
2	0.3	8-PSK
2	0.076	16-PSK

VLC System

By using (3.14), we have computed the average BER of VLC system considering BPSK modulation scheme for simplicity without loss of generality and the average BER expression is given by

$$BER_v = \frac{1}{2\sqrt{\pi}} \int_{\gamma_{\min}}^{\gamma_{\max}} F_{\gamma_v}(\gamma_v) \frac{e^{-\gamma_v/2}}{\sqrt{\gamma_v}} d\gamma_v, \tag{2.20}$$

By substituting (2.9) into (2.20), the integral can be simplified using the definition of the incomplete gamma function $\Gamma(a,x)$, as given in [45, Eq. (8.350.2)]. The final simplified expression is given by

$$\begin{aligned} BER_v = \frac{1}{2\sqrt{\pi}} \Bigg[& \mathscr{B}\Gamma\Big(\frac{1}{2}\Big)\Big(\Gamma\Big(\frac{1}{2},\gamma_{\min}\Big) - \Gamma\Big(\frac{1}{2},\gamma_{\max}\Big)\Big) \\ & + \Upsilon\Big(\Gamma\Big(\frac{m+1}{2m+6},\gamma_{\max}\Big) - \Gamma\Big(\frac{m+1}{2m+6},\gamma_{\min}\Big)\Big)\Bigg] \end{aligned} \tag{2.21}$$

IRS-Aided RF System

A similar CDF-based approach was adopted to compute the average BER of IRS-aided RF system considering BPSK scheme and the expression can be written as

$$BER_r = \frac{1}{2\sqrt{\pi}} \int_0^{\infty} \frac{F_{\gamma_r}(\gamma_r)}{\sqrt{\gamma_r}} e^{-\gamma_r/2} d\gamma, \tag{2.22}$$

By substituting (2.13) in (2.22), the above integral is simplified using integral by substitution technique followed by adopting Gauss Chebyshev quadrature technique from [45, Eq. (25.4.38)], to get the closed-form expression for average BER of the IRS-aided RF system, which is given by (2.23) on the top of next page, where Z is a Chebyshev parameter

and $\phi_i = \cos\left(\frac{(2i-1)\pi}{2Z}\right)$. Finally, the average BER of the hybrid system, assuming a hard-switching scheme, is computed by considering the average BER of the VLC system under non-outage conditions (i.e., by setting the limits of integration for the average BER of the VLC system from γ_{th} to $\gamma_{\max}$) and average BER of IRS-assisted RF system, which is given by

$$BER_r = \frac{1}{2\sqrt{\pi}}\left[\sqrt{\pi} - \frac{1}{\Gamma(a)}\frac{\pi}{Z}\sum_{i=1}^{Z}\sqrt{\frac{1-\phi_i^2}{4\left[\ln(2)-\ln(1+\phi_i)\right]}} \times \Gamma\left(a, \frac{1}{b}\sqrt{\frac{2\left[\ln(2)-\ln(1+\phi_i)\right]}{\bar{\gamma}_r}}\right)\right] \tag{2.23}$$

Now the final average BER of the proposed hybrid system is given by

$$\text{BER}_{\text{hybrid}} = BER_v + F_{\gamma_v}(\gamma_{\text{th}})\, BER_r \tag{2.24}$$

$$\begin{aligned} BER_{\text{hybrid}} = & \frac{1}{2\sqrt{\pi}}\left[\mathscr{B}\,\Gamma\left(\frac{1}{2}\right)\left(\Gamma\left(\frac{1}{2},\gamma_{\text{th}}\right)-\Gamma\left(\frac{1}{2},\gamma_{\max}\right)\right)\right. \\ & \left. + \Upsilon\left(\Gamma\left(\frac{m+1}{2m+6},\gamma_{\max}\right)-\Gamma\left(\frac{m+1}{2m+6},\gamma_{\text{th}}\right)\right)\right] \\ & + \frac{1}{2\sqrt{\pi}}\left[\mathscr{B} - \Upsilon\,\gamma_{\text{th}}^{-\frac{1}{m+3}}\right] \\ & \times \left[\sqrt{\pi} - \frac{\pi}{Z\Gamma(a)}\sum_{i=1}^{Z}\sqrt{\frac{1-\phi_i^2}{4\left(\ln(2)-\ln(1+\phi_i)\right)}}\right. \\ & \left. \times \Gamma\left(a, \frac{1}{b}\sqrt{\frac{2\left(\ln(2)-\ln(1+\phi_i)\right)}{\bar{\gamma}_{\text{r}}}}\right)\right] \end{aligned} \tag{2.25}$$

2.5 Results and Discussion

Table 2.2: VLC Simulation Parameters [4, 6, 47, 48]

Notation	Description	Value
$\phi_{1/2}$	LED semi-angle	40°
Ψ_{fov}	PD field of view	45°
n	Refractive index	1.5
m	Lambertian order parameter	2.60
L	Cell height	1.8 m
$r_{\max}$	Maximum cell radius	2 m
A_p	Area of photodetector	0.10 cm^2
R_p	Photodetector responsivity	0.74 A/W
$T(\psi)$	Optical filter gain	14.22 (Linear)
$G(\psi)$	Optical concentrator gain	4.5 (Linear)

Table 2.3: IRS-Aided RF Simulation Parameters [9, 47]

Notation	Description	Value
m_{rf}	Nakagami-m fading severity	2
Ω_{rf}	Nakagami-m shape parameter	1
N	Number of IRS elements	2

This section outlines the empirical evaluation and analytical results of the proposed hybrid RF/VLC system. All the analytical results are verified using the Monte-Carlo simulations and the flow diagrams of the simulation process are shown in Fig. 5.1 and 5.2 in Appendix. The analysis focuses into how different system configurations, reflected in the variability of key parameters, influence the primary performance metrics such as outage probability, average BER, and outage capacity. The hybrid system design integrates a primary VLC link with an IRS-aided RF backup link to augment communication reliability under varying indoor conditions. The VLC system, characterized by parameters mentioned in Table 2.2, operates under a Lambertian radiation pattern. Similarly, the IRS-aided RF system incorporates parameters including the number of IRS elements (N), Nakagami-m

fading severity parameter (m_{rf}), and the scaling parameter (Ω_{rf}), as outlined in Table 2.3. The threshold SNR for hard switching is considered to be 6 dB, as well as threshold capacity is taken as 5 dB. In addition, the hybrid system is evaluated under the assumption that the IRS is strategically positioned to optimally bridge the source and destination, thereby ensuring maximum efficacy in signal reflection and path optimization. By systematically altering these parameters, the simulations are designed to showcase the robustness of the system in maintaining communication quality across a spectrum of indoor environmental challenges.

Firstly, the optimum value of switching threshold SNR is computed using the numerical optimization method. To obtain the optimum value of threshold SNR, the average BER of hybrid system is plotted against the threshold SNR values in Fig. 2.4. We have considered three different values of the average SNR, i.e. 0 dB, 5 dB, and 10 dB. From Fig. 2.4, it is observed that at the threshold SNR values of 0 dB, 3 dB, and 6 dB corresponding to average SNR values of 0 dB, 5 dB, and 10 dB, respectively, the average SER of the hybrid system reaches its minimum for all three cases. Hence, these threshold values at which the average SER is minimized, are considered as the optimal threshold values. Note that, for the remainder of the manuscript, we have plotted the analytical results using the optimum threshold values obtained through the aforementioned numerical optimization technique.

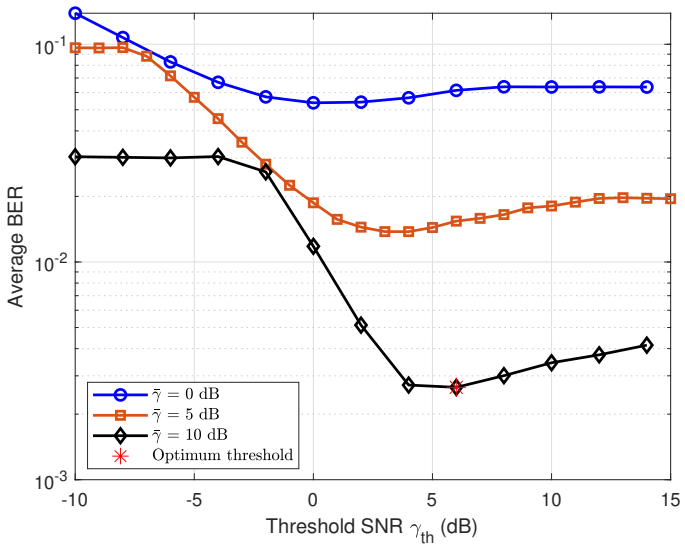

Figure 2.4: Average BER versus switching threshold γ_{th}.

Fig. 2.5 mainly compares the outage performance at an average SNR of 10 dB. The standalone VLC systems with maximum cell radii $r_{\max} = 3\,\text{m}$ and $r_{\max} = 2\,\text{m}$ exhibit outage probabilities of approximately 0.882443 and 0.579632, respectively, highlighting the influ-

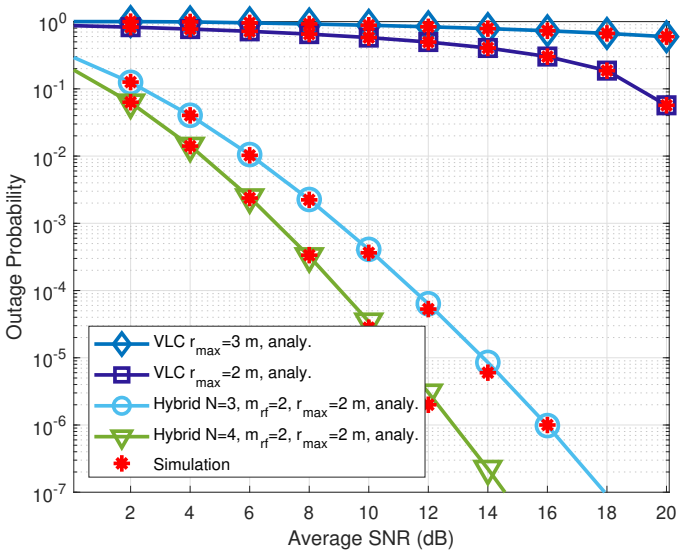

Figure 2.5: Outage probability of VLC and hybrid system varying r_{max} and N.

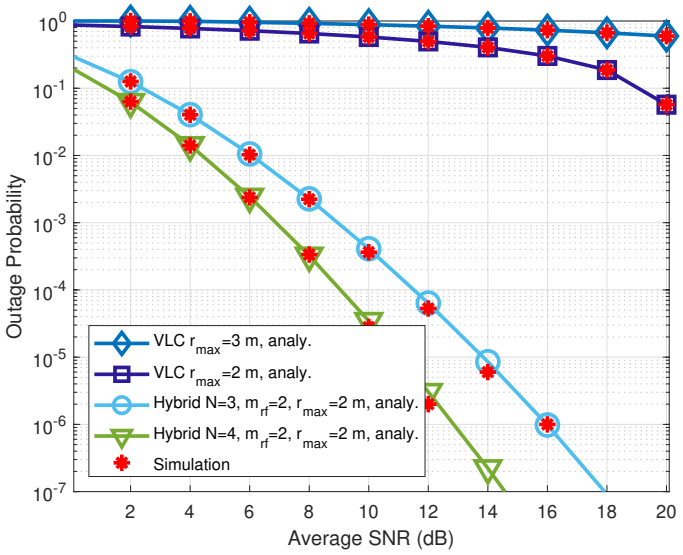

Figure 2.6: Outage probability of VLC and hybrid system varying R_p and N.

ence of cell radius on communication reliability. The hybrid configurations significantly improve outage performance even further. The system with $N = 3$, $m_{\text{rf}} = 2$, and $r_{\text{max}} = 2\,\text{m}$ achieves a lower outage probability of 0.000364 at the same SNR level. Additionally, the more advanced hybrid system with $N = 4$, $m_{\text{rf}} = 2$, and $r_{\text{max}} = 2\,\text{m}$ further reduces the outage probability to 0.000028, showing a significant enhancement over the $N = 3$ configuration.

Fig. 2.6 illustrates the outage probability versus average SNR for our hybrid RF/VLC system, evaluated under the parameters detailed in Tables 2.2 and 2.3. We present two VLC outage probability curves for photodiode responsivities $R_p = 0.74\,\text{A/W}$ and $R_p = 0.84\,\text{A/W}$.

The latter configuration shows superior performance compared to the former. We also explore the hybrid system configurations with $N = 2$, $m_{\text{rf}} = 2$ and $N = 4$, $m_{\text{rf}} = 3$, both using $R_p = 0.84\,\text{A/W}$. At 20 dB, the standalone VLC system with $R_p = 0.84\,\text{A/W}$ demonstrates an outage probability of 0.056859. Comparatively, the hybrid system with $N = 2$ and $m_{\text{rf}} = 2$ achieves a similar outage probability at a reduced SNR of 7.5 dB, indicating an SNR gain of 12.5 dB over the standalone VLC system. The configuration with $N = 4$ and $m_{\text{rf}} = 3$ attains this outage probability at an even lower SNR of 4.5 dB, representing a total SNR gain of 15.5 dB compared to the standalone system, and an additional 3 dB over the $N = 2$ configuration. These results suggest that enhancing the number of IRS elements and increasing the Nakagami-m fading severity parameter, along with the photodetector responsivity, significantly improves the overall performance of the hybrid system for demanding applications.

Fig. 2.7 illustrates the outage probability as a function of average SNR for both standalone VLC systems and hybrid VLC/IRS-aided RF systems under different values of photodiode areas. At an SNR of 20 dB, the standalone VLC systems exhibit significant differences in outage probability with photodiode areas: the system with $A_p = 0.1\,\text{cm}^2$ has an outage probability of approximately 0.64813, while the system with $A_p = 0.20\,\text{cm}^2$ shows a reduced outage probability of 0.4488. In contrast, the hybrid system configurations demonstrate markedly enhanced performance. Specifically, the configuration with $N = 2$ and $m_{\text{rf}} = 2$ achieves an outage probability of 1.46×10^{-6} at an SNR of 20 dB. Remarkably, the more advanced setup with $N = 4$ and $m_{\text{rf}} = 3$ attains a similar low outage probability but at a significantly lower SNR of 8 dB, indicating a substantial SNR gain of 12 dB compared to $N = 2$ configuration. As evident in Figs. 2.5–2.7, combining an IRS-assisted RF subsystem with VLC substantially reduces outage probability by offering multi-layer diversity and mitigating severe fading. Optimizing key parameters (e.g., the number of IRS elements, Nakagami-m, photodiode responsivity, and cell radius) enhances effective signal gain and alleviates path loss, thereby yielding markedly improved reliability and reducing outage probabilities across diverse channel conditions.

Fig. 2.8 illustrates the average BER performance across various configurations at increasing levels of average SNR. The standalone VLC systems with $r_{\max} = 2.2\,\text{m}$ and $r_{\max} = 1.8\,\text{m}$ show notable differences in BER, with the smaller cell radius offering better performance. Specifically, at 20 dB, the BER for $r_{\max} = 1.8\,\text{m}$ is significantly lower at 0.0002226 compared to 0.002226 for $r_{\max} = 2.2\,\text{m}$. In the hybrid system configurations, we see a sub-

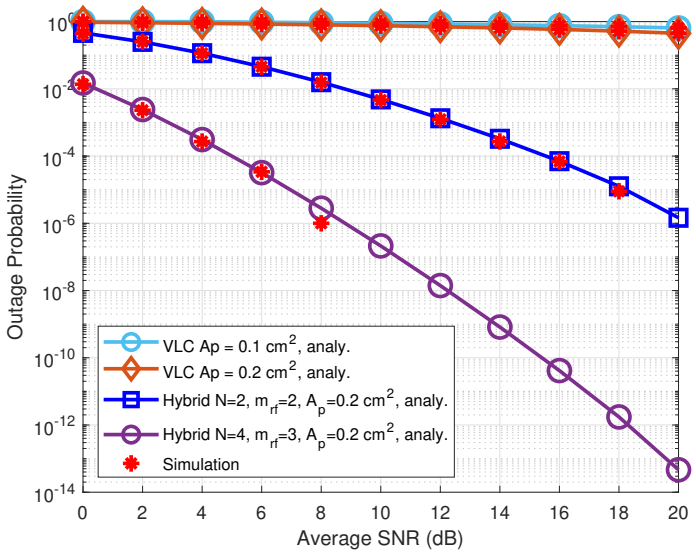

Figure 2.7: Outage probability of VLC and hybrid system varying A_p, N and m_{rf}.

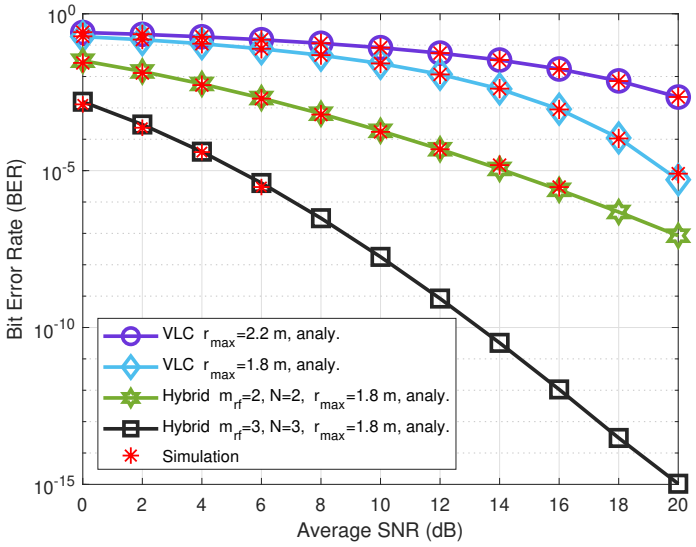

Figure 2.8: BER for VLC and hybrid system varying m_{rf}, N and r_{max}.

stantial enhancement in BER performance. For $N = 2$, $m_{\text{rf}} = 2$, and $r_{\text{max}} = 1.8\,\text{m}$, the BER at 15 dB is approximately similar to that of the VLC performance at 20 dB indicating an SNR gain of 5 dB. This is further improved in the $N = 3$, $m_{\text{rf}} = 3$, and $r_{\text{max}} = 1.8\,\text{m}$ configuration, where the BER drops to an extremely low 3×10^{-6} at just 4 dB, highlighting the SNR gain of 16 dB compared to the VLC system.

Fig. 2.9 presents the BER performance analysis of the proposed hybrid VLC/IRS-aided RF system compared with standalone VLC systems under variations in photodiode responsivity R_p and IRS element configurations. For the standalone VLC systems, the BER is

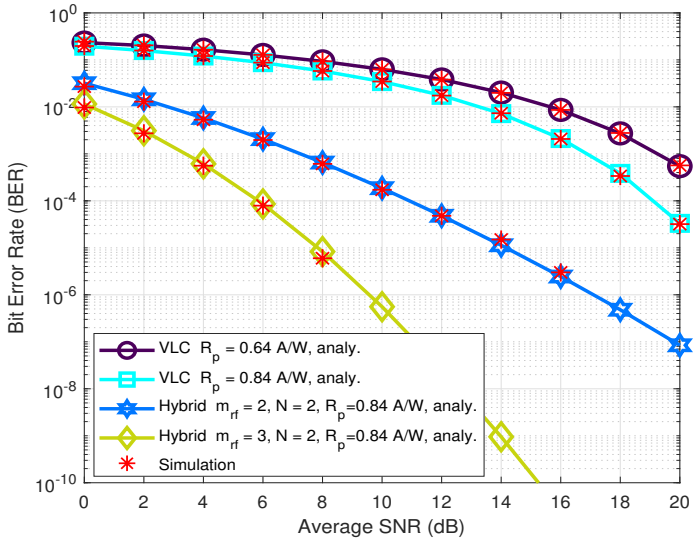

Figure 2.9: BER for VLC and hybrid system varying m_{rf} and R_p.

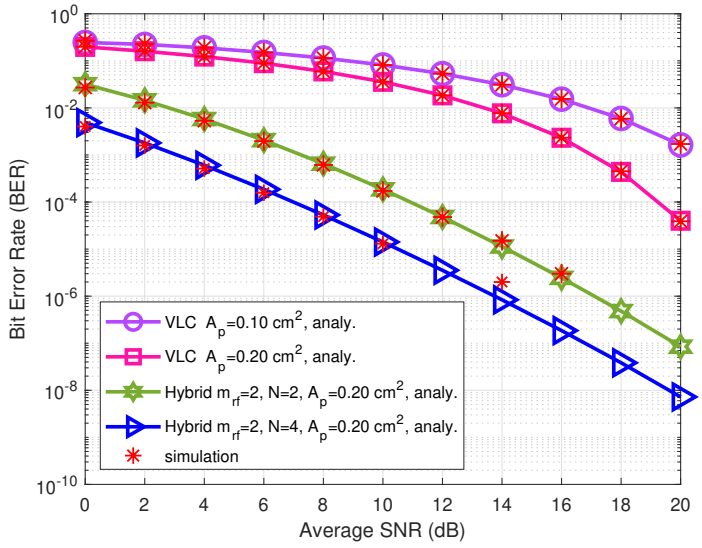

Figure 2.10: BER for VLC and hybrid system varying A_p and N.

plotted for two different responsivities, $R_p = 0.64\,\text{A/W}$ and $R_p = 0.84\,\text{A/W}$, showing enhanced BER performance as responsivity increases. At an SNR of 20 dB, the BER for $R_p = 0.64\,\text{A/W}$ registers approximately 0.000547663, improving significantly to 0.0003226 for $R_p = 0.84\,\text{A/W}$.

In the hybrid system configurations, the performance with $m_{\text{rf}} = 3$, $N = 2$, and $R_p = 0.84\,\text{A/W}$ further augments BER effectiveness. The hybrid setup achieves an average BER near that of the standalone VLC system with $R_p = 0.84\,\text{A/W}$ at 12 dB, showcasing an SNR

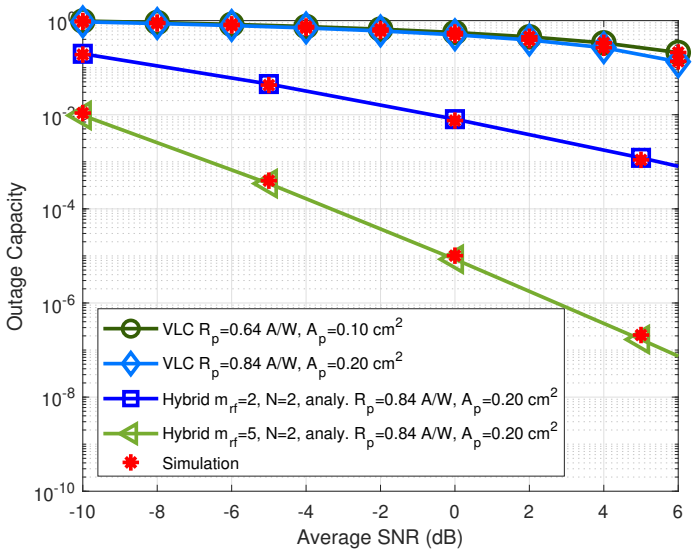

Figure 2.11: Outage capacity comparison of VLC and hybrid system.

gain of approximately 8 dB. Additionally, increasing IRS elements to $N = 4$ under the same conditions yields an even lower BER at just 4 dB, indicating a remarkable total SNR gain of 16 dB compared to the standalone VLC system with $R_p = 0.84$ A/W.

Fig. 2.10 showcases the BER performance of the proposed hybrid VLC/IRS-aided RF system in comparison with standalone VLC systems under varying photodiode area (A_p) and IRS element configurations. For standalone VLC systems, the BER is plotted for two photodiode areas, $A_p = 0.10\,\text{cm}^2$ and $A_p = 0.20\,\text{cm}^2$, exhibiting better BER performance as the area increases. At 20 dB, the BER for $A_p = 0.10\,\text{cm}^2$ is approximately 0.001709, while for $A_p = 0.20\,\text{cm}^2$, it significantly improves to 0.0001709.

The hybrid system configurations assuming, $m_{\text{rf}} = 2$ with $N = 2$ and $N = 4$ IRS elements both using $A_p = 0.20\,\text{cm}^2$, demonstrate further enhanced BER performance. At 12 dB, the system with $N = 2$ IRS elements achieves a BER close to that of the standalone VLC system with $A_p = 0.20\,\text{cm}^2$, showing an SNR gain of 8 dB. More impressively, the configuration with $N = 4$ IRS elements achieves a comparable BER at just 4 dB, reflecting an additional SNR gain of 8 dB over $N = 2$ configuration, and totaling 16 dB compared to the standalone VLC system. This indicates that increasing the number of IRS elements significantly improves the system's performance by leveraging enhanced signal focusing and reflection capabilities provided by the IRS technology.

These findings, presented in Fig. 9, affirm the potential of integrating IRS technology to substantially boost the BER performance of hybrid RF/VLC systems. The ability of the

hybrid system to achieve comparable or superior BER metrics at lower SNRs showcases the IRS's effectiveness in enhancing signal quality, particularly under challenging communication conditions. This demonstrates that intelligent system configurations, combining increased photodetector areas with strategic IRS usage, can significantly transcend the performance boundaries of traditional VLC systems. As depicted in Figs. 2.8–2.10, incorporating an IRS-assisted RF link into a VLC system markedly reduces the BER by exploiting enhanced channel gains. By strategically optimizing key parameters—such as the number of IRS elements, photodiode responsivity/area, and cell radius—the hybrid configuration mitigates the channel distortions more effectively than standalone VLC. Consequently, the system achieves significantly lower BER at reduced SNR values, affirming the substantial advantages of intelligently combining IRS technology with VLC.

Fig. 2.11 presents a comparative analysis of the outage capacity between the standalone VLC system and the hybrid system against average SNR values. For the standalone VLC system at an SNR of 6 dB, when the photodiode responsivity and area are set to $R_p = 0.64$ A/W and $A_p = 0.10$ cm^2, respectively, the outage capacity is approximately 0.21. Increasing the responsivity and area to $R_p = 0.84$ A/W and $A_p = 0.20$ cm^2 improves the performance, reducing the outage capacity to 0.14. In contrast, the hybrid VLC/IRS-aided RF system demonstrates a significant reduction in outage capacity due to the improved diversity gain and optimized signal reflections enabled by the IRS. With $m_{\text{rf}} = 2$, $N = 2$ IRS elements, and analytically computed values, the outage capacity at 6 dB SNR drops to 0.00109. Further enhancing the RF link by increasing m_{rf} to 5 results in a dramatic improvement, bringing the outage capacity down to 2.08×10^{-7}. These results highlight that the hybrid system significantly outperforms the standalone VLC system, particularly in low SNR scenarios, demonstrating the advantage of IRS-assisted RF links in mitigating fading effects and improving overall system reliability.

2.6 Conclusion and Future Work

In this paper, we proposed an IRS-aided hybrid RF/VLC system to enhance indoor communication performance, addressing traditional VLC limitations such as non-LoS conditions and physical obstructions. The system integrates a primary VLC link with an IRS-aided RF backup link, employing a hard-switching mechanism to activate the RF link when the

instantaneous SNR of VLC link falls below a predefined threshold. Analytical models were developed to derive the closed-form expressions for key performance metrics, including outage probability, BER, and outage capacity, considering Lambertian radiation for VLC and Nakagami-*m* fading for RF channels. Monte-Carlo simulations were conducted to validate the theoretical results. From the numerical results, it was observed that the proposed hybrid VLC/IRS-assisted RF system demonstrated significant improvements over standalone VLC system in terms of outage probability, average BER, and outage capacity under different system and channel parameters. Future work will focus on enhancing adaptability through machine learning algorithms, exploring scalability in complex indoor environments, and optimizing IRS configurations for improved wave propagation control. These advancements aim to meet the evolving demands of modern indoor communication systems.

Chapter 3

Hybrid VLC/THz Communication Systems

3.1 Introduction

The exponential growth in data traffic and the increasing demand for high-speed, low-latency indoor communication have prompted researchers to explore hybrid communication architectures that transcend the limitations of individual wireless technologies. VLC leveraging the unlicensed optical spectrum, provides high data rates and security, making it suitable for indoor environments with dense user deployments [1, 2]. However, its performance is significantly constrained by the need for LoS propagation and susceptibility to shadowing and ambient light interference [3, 14].

THz communication, on the other hand, offers unprecedented bandwidth availability and is poised as a key technology for beyond-5G and 6G systems [49, 7]. Despite this potential, the THz band suffers from severe propagation losses, high molecular absorption, and antenna misalignment issues, which challenge its practical deployment [18, 19, 29]. Furthermore, the performance degradation caused by hardware impairments in THz transceivers cannot be ignored [34, 35].

To address the shortcomings of VLC and THz systems, a hybrid VLC/THz architecture is proposed. This hybrid framework aims to exploit the high capacity and coverage of THz links while retaining the advantages of VLC in scenarios where LoS conditions prevail. Such a system dynamically switches or aggregates communication links based on channel state information, thereby improving reliability, coverage, and throughput in complex indoor

environments [4, 5, 50].

This chapter presents the modeling and performance analysis of a hybrid VLC/THz communication system. Theoretical models for both VLC and THz channels are developed, and their joint performance is analyzed under realistic fading, alignment, and noise conditions. The results validate the effectiveness of the hybrid strategy in achieving enhanced quality of service (QoS) compared to standalone VLC or THz systems.

3.2 Organisation of Chapter

The remainder of this chapter is structured as follows: Section 3.3 details the overall system model, including the architecture of the hybrid system and communication flow between the VLC and THz components. Section 3.3.1 elaborates on the THz channel model with emphasis on path loss, molecular absorption, and antenna misalignment effects. Section 3.3.2 extends the model to incorporate practical hardware impairments and stochastic fading conditions observed in real-world THz systems.

Section 3.4 presents the analytical performance analysis of the hybrid system, focusing on outage probability, outage capacity, and average BER under various channel scenarios. Section 3.5 discusses the simulation results and compares them with the theoretical expressions to validate the model. Finally, Section 3.6 concludes the chapter by summarizing key findings and proposing future directions for optimizing hybrid VLC/THz systems.

3.3 System Model

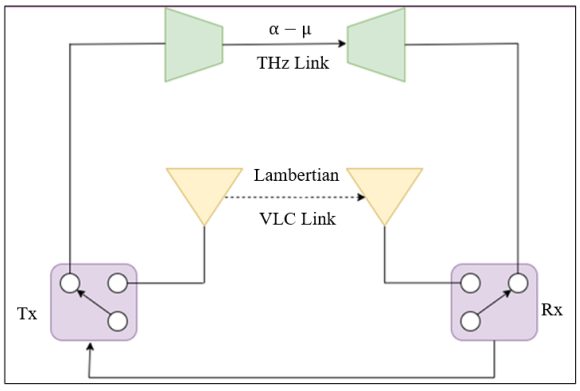

Figure 3.1: Hybrid VLC/THz system model

In the THz system, the channel coefficient h is modeled as a composite product of three independent channel effects, which include path gain h_l, pointing error h_p, and small-scale fading h_f [51], and it can be written as

$$h = h_l h_p h_f. \tag{3.1}$$

Pointing Error Model

The PDF of pointing errors, which is useful in modelling the beam misalignment, is given by [52, eq. (22)]

$$f_{h_p}(h_p) = \frac{\zeta_1}{A_0}\left(\frac{h_p}{A_0}\right)^{\zeta_1^2-1}, \tag{3.2}$$

where $\zeta_1 = \frac{w_{\text{eq}}}{2\sigma_i}$ is the pointing error coefficient, w_{eq} is the equivalent beam waist, σ_i is the jitter deviation, and A_0 is the fraction of collected power at the receiver.

Path Gain Model

The path gain h_l is modeled as [52, eq. (6)]

$$f_{h_l}(h_l) = \frac{c\sqrt{G_t G_r}}{4\pi f d}\exp\left(-\frac{1}{2}k_a(f)d\right), \tag{3.3}$$

where G_t and G_r are the transmitter and receiver antenna gains, f is the operating frequency, d is the link distance, c is the speed of light, and $k_a(f)$ is the molecular absorption coefficient.

Fading Model (Generalized α-μ Distribution)

The multipath fading h_f follows a generalized α-μ distribution, whose PDF is given by [52, eq. (24)]

$$f_{h_f}(h_f) = \frac{\alpha\mu^{\mu}}{\hat{h}_f^{\alpha\mu}\Gamma(\mu)}h_f^{\alpha\mu-1}\exp\left(-\frac{\mu h_f^{\alpha}}{\hat{h}_f^{\alpha}}\right), \tag{3.4}$$

where α is the fading parameter, μ is the normalized variance of the fading envelope, $\hat{h}_f$ is the α-root mean value, and $\Gamma(\cdot)$ is the gamma function.

Joint Distribution of $|h_{fp}| = |h_f||h_p|$

The combined PDF of fading and pointing error is obtained using the random variable transformation as

$$f_{|h_{fp}|}(x) = \zeta_1^2 A_0^{-\zeta_1^2}\frac{\mu^{\alpha}\zeta_1^2}{\hat{h}_f^{\alpha\mu}\Gamma(\mu)}x^{\zeta_1^2-1}\Gamma\left(\frac{\alpha\mu-\zeta_1^2}{\alpha}, \frac{\mu x^{\alpha}A_0^{-\alpha}}{\hat{h}_f^{\alpha}}\right), \tag{3.5}$$

where $\Gamma(\cdot,\cdot)$ is the upper incomplete gamma function.

Instantaneous SNR of the THz Link

Now the instantaneous SNR γ_t at the receiver is given by

$$\gamma_t = h_l^2 |h_{fp}|^2 \bar{\gamma}_t, \tag{3.6}$$

where $\bar{\gamma}_t$ is the average SNR.

By transformation of variables, the PDF of γ_t is derived as

$$f_{\gamma_t}(\gamma_t) = \frac{\zeta_1^2 A_0^{-\zeta_1^2} \mu^\alpha \zeta_1^2 \gamma_t^{\frac{\zeta_1^2}{2}-1}}{2\hat{h}_f^\alpha \Gamma(\mu) \bar{\gamma}_t^{\frac{\zeta_1^2}{2}}} \Gamma\left(\frac{\alpha\mu - \zeta_1^2}{\alpha}, \frac{\mu \gamma_t^{\frac{\alpha}{2}} A_0^{-\alpha}}{\hat{h}_f^\alpha \bar{\gamma}_t^{\frac{\alpha}{2}}}\right), \tag{3.7}$$

CDF of the THz Instantaneous SNR

By integrating the obtained PDF, the the corresponding CDF of instantaneous SNR is given by

$$F_{\gamma_t}(\gamma_t) = 1 - \frac{\zeta_1^2 A_0^{-\zeta_1^2} \gamma_t^{\frac{\zeta_1^2}{2}} h_l^{-\zeta_1^2}}{\hat{h}_f^\alpha \alpha \bar{\gamma}_t^{\frac{\zeta_1^2}{2}}} \sum_{k=0}^{\mu-1} \frac{\mu^\alpha \zeta_1^2}{k!} \Gamma\left(\frac{\alpha k - \zeta_1^2}{\alpha}, \frac{\mu \gamma_t^{\frac{\alpha}{2}} A_0^{-\alpha}}{\hat{h}_f^\alpha \bar{\gamma}_t^{\frac{\alpha}{2}} h_l^\alpha}\right). \tag{3.8}$$

This model comprehensively accounts for all key degrading effects present in the THz link path loss, beam misalignment, and multipath fading thus forming the analytical foundation for evaluating THz system performance in hybrid optical–wireless communication scenarios.

3.4 Performance Analysis

This section presents the performance analysis of hybrid VLC/THz system. The expressions for the outage probability, outage capacity and average BER are derived for the proposed system considering hard-switching scheme.

3.4.1 Outage Probability

Outage probability is a key performance indicator in communication systems, quantifying the likelihood that the instantaneous SNR falls below a predefined threshold, γ_{th}, leading to

a communication failure. When the instantaneous SNR of the VLC link falls below γ_{th}, the system switches to the backup THz link using a hard-switching strategy.

Therefore, the outage probability of the hybrid system is defined as the probability that both the VLC and THz links simultaneously fail to maintain the SNR above γ_{th}. Mathematically, the outage probability can be expressed as

$$P_{\text{out}} = F_{\gamma_v}(\gamma_{th}) F_{\gamma_t}(\gamma_{th}), \tag{3.9}$$

where $F_{\gamma_v}(.)$ and $F_{\gamma_t}(.)$ are the CDFs of the instantaneous SNRs of the VLC and THz links, respectively. These functions are evaluated at the outage threshold γ_{th}. The CDF of the VLC link is given by (2.9).

Substituting the expressions of the CDFs, the final closed-form expression for the outage probability of the hybrid VLC/THz system is written as:

$$P_{\text{out}} = \left(\mathscr{B} - \Upsilon \gamma_{th}^{-\frac{1}{m+3}} \right) \left[1 - \frac{\zeta_1^2 A_0^{-\zeta_1^2} \gamma_{th}^{\frac{\zeta_1^2}{2}} h_l^{-\zeta_1^2}}{\hat{h}_f^{\alpha} \alpha \bar{\gamma}_t^{\frac{\zeta_1^2}{2}}} \sum_{k=0}^{\mu-1} \frac{\mu^{\alpha} \zeta_1^2}{k!} \Gamma \left(\frac{\alpha k - \zeta_1^2}{\alpha}, \frac{\mu \gamma_{th}^{\frac{\alpha}{2}} A_0^{-\alpha}}{\hat{h}_f^{\alpha} \bar{\gamma}_t^{\frac{\alpha}{2}} h_l^{\alpha}} \right) \right]. \tag{3.10}$$

3.4.2 Outage Capacity

Outage capacity measures the probability that the normalized capacity of the communication system falls below a predefined threshold, denoted as C_{th}. The normalized capacity for a given instantaneous SNR γ is expressed as [46]

$$C_{\text{norm}} = \log_2(1+\gamma) \tag{3.11}$$

Now, the outage capacity of the hybrid system is given by

$$\begin{aligned} C_{\text{out}} &= \Pr\left(\log_2(1+\gamma_v) \leq C_{\text{th}} \cap \log_2(1+\gamma_t) \leq C_{\text{th}}\right) \\ &= \Pr\left(\gamma_v \leq 2^{C_{\text{th}}} - 1 \cap \gamma_t \leq 2^{C_{\text{th}}} - 1\right) \\ &= F_{\gamma_v}(2^{C_{\text{th}}} - 1) F_{\gamma_t}(2^{C_{\text{th}}} - 1) \end{aligned} \tag{3.12}$$

From (3.12), and using the expressions for the CDFs of the VLC and THz links, the final

analytical expression for the outage capacity of the hybrid VLC/THz system is given by

$$C_{\text{out}} = \left(\mathscr{B} - \Upsilon\,(2^{C_{\text{th}}}-1)^{-\frac{1}{m+3}}\right) \times \left[1 - \frac{\zeta_1^2 A_0^{-\zeta_1^2}(2^{C_{\text{th}}}-1)^{\frac{\zeta_1^2}{2}} h_l^{-\zeta_1^2}}{\hat{h}_f^{\alpha}\alpha\bar{\gamma}_t^{\frac{\zeta_1^2}{2}}} \sum_{k=0}^{\mu-1} \frac{\mu^{\alpha}\zeta_1^2}{k!}\Gamma\left(\frac{\alpha k-\zeta_1^2}{\alpha}, \frac{\mu(2^{C_{\text{th}}}-1)^{\frac{\alpha}{2}}A_0^{-\alpha}}{\hat{h}_f^{\alpha}\bar{\gamma}_t^{\frac{\alpha}{2}}h_l^{\alpha}}\right)\right] \tag{3.13}$$

3.4.3 Average BER

We assume sub-carrier intensity-modulation-based MPSK for VLC and THz communication. The generalized governing SER expression for MPSK modulation scheme for a given instantaneous SNR γ has been utilized to calculate the average SER using the CDF-based approach and is given by

$$P_{\text{ser}} = \frac{t\sqrt{u}}{2\sqrt{2\pi}} \int_0^{\infty} \frac{F_{\gamma}(\gamma)}{\sqrt{\gamma}} e^{-\frac{u\gamma}{2}} d\gamma, \tag{3.14}$$

where $F_{\gamma}(\gamma)$ indicates the CDF of either VLC or RF link, t and u indicate modulation specific parameters as shown in Table 2.1. These parameters can be varied to obtain the average SER of the required MPSK signalling scheme.

VLC System

We have already derived the final closed-form expression for the average BER of VLC system in (2.21).

THz System

A similar CDF-based approach was adopted to compute the average BER of THz system considering BPSK scheme and the expression can be written as

$$BER_t = \frac{1}{2\sqrt{\pi}} \int_0^{\infty} \frac{F_{\gamma_t}(\gamma_t)}{\sqrt{\gamma_t}} e^{-\gamma_t/2} d\gamma, \tag{3.15}$$

By substituting (3.8) in (3.15), the above integral is complex in nature and hence, we solve the same using the Gauss-Laguerre quadrature technique [53], to get the closed-form expression for average BER of the THz system, which is given by

$$\text{BER}_t \approx \frac{1}{4\Gamma(0.5)} \sum_{l=1}^{J} w_l f(x_l) + E_J \tag{3.16}$$

where w_l are the associated weights and x_l is the l^{th} root of the Laguerre polynomial. Now, the final average BER of the proposed hybrid system is given by (3.18)

$$\text{BER}_{\text{hybrid}} = \text{BER}_v + F_{\gamma_v}(\gamma_{\text{th}})\,\text{BER}_t \tag{3.17}$$

$$\begin{aligned}\text{BER}_{\text{hybrid}} =& \frac{1}{2\sqrt{\pi}}\Bigg[\mathscr{B}\Gamma\Big(\frac{1}{2}\Big)\Big(\Gamma\Big(\frac{1}{2},\gamma_{\text{th}}\Big)-\Gamma\Big(\frac{1}{2},\gamma_{\max}\Big)\Big)\\ &+\Upsilon\Big(\Gamma\Big(\frac{m+1}{2m+6},\gamma_{\max}\Big)-\Gamma\Big(\frac{m+1}{2m+6},\gamma_{\text{th}}\Big)\Big)\Bigg]\\ &+\Big(\mathscr{B}-\Upsilon\,\gamma_{\text{th}}^{-\frac{1}{m+3}}\Big)\Bigg[\frac{1}{4\Gamma(0.5)}\sum_{l=1}^{J} w_l f(x_l)+E_J\Bigg]\end{aligned} \tag{3.18}$$

3.5 Results and Discussion

This section presents the simulation setup, empirical evaluation, and analytical verification of the proposed hybrid VLC/THz communication system. The system's performance is evaluated using both closed-form analytical expressions and Monte Carlo simulations to validate theoretical claims. Unless otherwise stated, the parameters for the VLC system are adopted from Chapter 2, specifically Table 2.2, which defines the photodetector area, semi-angle at half power, and other optical channel parameters under the Lambertian radiation pattern.

For the THz link, the generalized α–μ fading model is used to capture the channel behavior, with fading parameters set to $\alpha = \{2,4\}$ and $\mu = \{1,2\}$ in accordance with prior literature. These values allow us to study the impact of varying channel severity and path loss on system reliability. The threshold SNR for hard-switching between VLC and THz links is taken as 6 dB, while the threshold for outage capacity is set to 5 dB. Fig. 3.2 illustrates the outage probability versus average SNR performance for the VLC and hybrid VLC/THz systems. The standalone VLC system, operating with parameters $r_{\max} = 2\,\text{m}$ and $R_p = 0.64\,\text{A/W}$, exhibits significantly higher outage probability across the SNR range. At 20 dB, the standalone VLC system yields an outage probability of approximately 0.597537. In

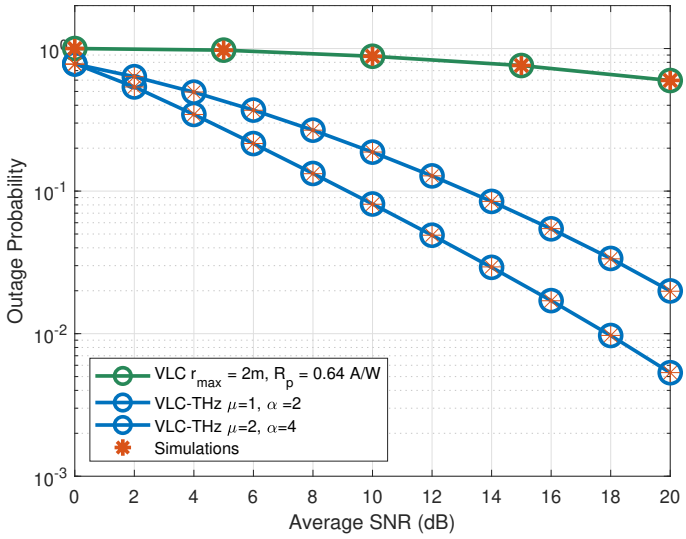

Figure 3.2: Outage probability of VLC and hybrid VLC-THz System

contrast, the hybrid VLC/THz system achieves notably lower outage probabilities, depending on the α and μ fading parameters of the THz link. For example, under the configuration $\mu = 1$, $\alpha = 2$, the hybrid system achieves an outage probability of approximately 0.0199448 at 20 dB. This represents a dramatic improvement over the standalone VLC system, amounting to an SNR gain of over 15 dB for the same outage level. Further enhancement is observed for the case $\mu = 2$, $\alpha = 4$, where the hybrid system achieves an outage probability as low as 0.017014 at 16 dB, showcasing improved robustness due to stronger fading conditions. These results highlight the performance advantage of integrating a THz link as a backup, especially under severe channel conditions, and demonstrate how tuning the α and μ parameters can significantly improve the system's outage behavior.

Fig. 3.3 presents the BER versus average SNR for the standalone VLC system and the proposed hybrid VLC/THz systems under varying α and μ parameters of the THz link. The standalone VLC system, configured with a photodetector area of $A_p = 0.10\,\text{cm}^2$, achieves an average BER of approximately 0.034595 at 20 dB SNR. The first hybrid configuration, with $\mu = 1$ and $\alpha = 2$, attains this same BER at a reduced SNR of approximately 12 dB, yielding an SNR gain of 8 dB over the standalone VLC system. A further enhancement is observed with the second hybrid configuration, where $\mu = 2$ and $\alpha = 4$. This setup achieves the same BER of 0.034595 at an even lower SNR of 6 dB, resulting in a total SNR gain of 14 dB over the VLC-only system, and an additional 6 dB improvement compared to the $\mu = 1$, $\alpha = 2$ configuration. These results validate the performance benefits of integrating

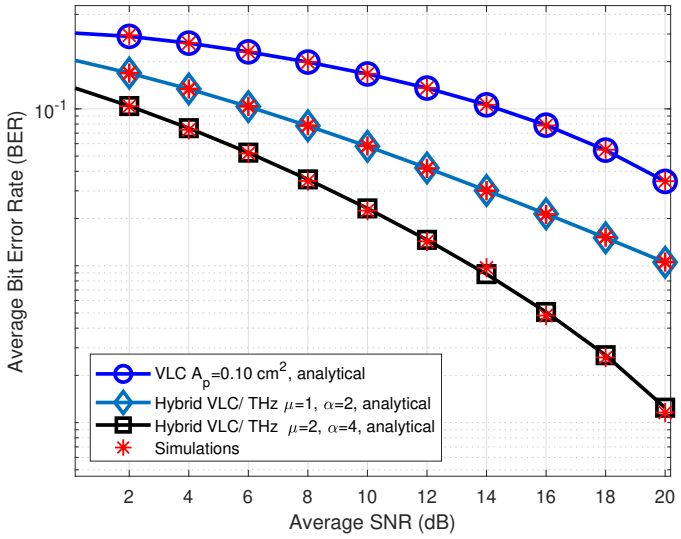

Figure 3.3: Average BER of VLC and hybrid VLC-THz System

a THz backup link with the VLC system and emphasize the importance of optimizing the α-μ fading parameters for achieving superior error performance in hybrid communication scenarios.

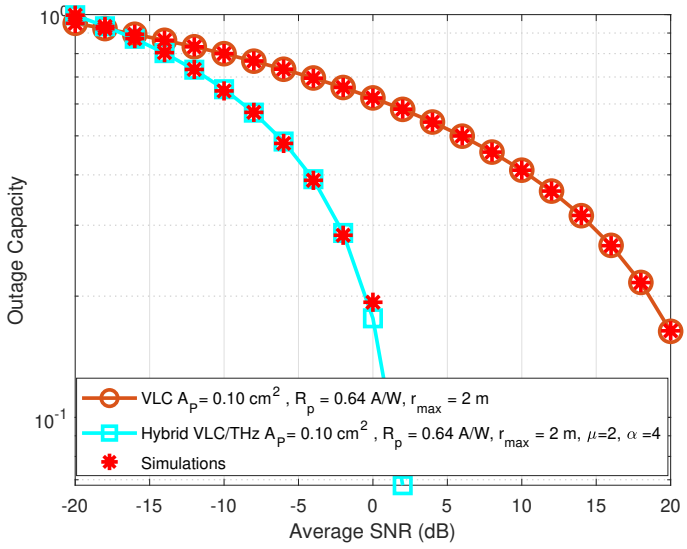

Figure 3.4: Outage Capacity of VLC and hybrid VLC-THz System

Fig. 3.4 depicts the outage capacity versus average SNR for both the standalone VLC system and the hybrid VLC/THz system under identical photodetector and channel parameters. The VLC system, operating with $A_p = 0.10\,\text{cm}^2$, $R_p = 0.64\,\text{A/W}$, and $r_{\max} = 2\,\text{m}$, achieves an outage capacity of approximately 0.317239 at 14 dB. In comparison, the hybrid

VLC/THz configuration employing the same VLC parameters but augmented with a THz backup link characterized by $\mu = 2$ and $\alpha = 4$ achieves nearly the same outage capacity value of 0.283264 at a significantly lower SNR of -2 dB. This result translates to an SNR gain of 16 dB, underscoring the hybrid system's efficiency in maintaining capacity performance even under highly degraded SNR conditions. These findings strongly validate the advantage of incorporating a THz link as a backup to the VLC system, particularly in scenarios demanding capacity assurance under fading or blockage-prone environments. The observed improvement is attributed to the robustness of the α-μ faded THz channel, which compensates effectively for the limitations of the VLC channel.

3.6 Conclusion and Future Work

In this chapter, we proposed a hybrid VLC/THz communication system to address the performance limitations of standalone VLC links in environments affected by non-LoS conditions, dynamic channel variations, and restricted coverage. The system employs a hard-switching mechanism, where a backup THz link is activated when the instantaneous SNR of the VLC link falls below a predefined threshold. The VLC link was modeled using Lambertian radiation characteristics, while the THz channel followed an α-μ fading model to capture the small-scale signal fluctuations typical of high-frequency bands. Closed-form analytical expressions were derived for key performance metrics including outage probability, average BER, and outage capacity. Gauss–Laguerre quadrature was employed to efficiently compute the BER under complex fading conditions. Monte-Carlo simulations were used to verify the accuracy of the analytical results. Numerical evaluations showed that the proposed hybrid VLC/THz system significantly outperforms the standalone VLC system, especially in challenging scenarios. Notably, the system exhibited substantial SNR gains in both BER and outage performance, demonstrating its effectiveness in enhancing link reliability and capacity in next-generation wireless networks.

Future work will explore the integration of adaptive link selection mechanisms using machine learning to further optimize switching decisions between VLC and THz links. Additional focus will be placed on joint beam alignment, mobility modeling, and real-time CSI acquisition for the THz channel. Expanding the system to support multi-user and multi-hop hybrid VLC/THz topologies will also be investigated to ensure scalability and robustness in

complex deployment scenarios, including smart factories and indoor vehicular communications.

Chapter 4

Hybrid VLC/IRS-Aided THz Communication Systems

4.1 Introduction

The increasing demand for ultra-reliable, high-capacity indoor wireless communication has led to the exploration of hybrid communication systems that combine multiple complementary technologies. VLC offers high data rates and immunity to electromagnetic interference by utilizing the optical spectrum, making it well-suited for indoor applications [1, 2]. However, VLC systems are inherently limited by LoS constraints and are highly sensitive to obstacles and ambient lighting [3, 14].

The THz band, with its immense spectrum availability, promises extremely high data rates and is a prime candidate for B5G and 6G applications [7, 49]. Despite this, THz systems suffer from severe propagation losses, beam misalignment due to the use of highly directive antennas, and performance degradation due to hardware imperfections [18, 29, 35]. These challenges hinder the standalone deployment of THz systems in complex indoor settings.

RIS or IRS have emerged as a transformative technology capable of overcoming channel impairments by dynamically controlling the propagation environment. IRS can reflect incident signals toward desired directions by adjusting the phase shifts of passive elements, thus improving link reliability and spectral efficiency [9, 16]. While IRS has been widely studied in the context of RF and VLC systems [10, 17], its application in the THz domain is still underexplored.

This chapter introduces a hybrid VLC/IRS-aided THz communication system, designed to harness the advantages of VLC for LoS-dominant short-range links, while leveraging the wide bandwidth of the THz band, enhanced by IRS for improved reliability and coverage. The system employs a hard-switching mechanism based on signal quality, where the IRS-aided THz link serves as a robust backup to the VLC link in obstructed scenarios. This hybrid integration promises significant improvements in performance metrics such as outage probability and average BER, while addressing the fundamental limitations of each individual technology.

4.2 Organisation of Chapter

The rest of this chapter is organized as follows: Section 4.1 introduces the motivation and relevance of combining VLC with IRS-aided THz communication. Section 4.3 outlines the hybrid system model, detailing the interaction between the VLC link and the IRS-assisted THz link. Section 4.3.1 presents the THz channel model, emphasizing propagation loss, molecular absorption, and antenna misalignment. Section 4.3.2 further incorporates IRS behavior and its impact on the THz channel, including phase shift design and reflection geometry.

Section 4.4 provides a comprehensive performance analysis, including closed-form derivations of outage probability and average BER under composite VLC and IRS-aided THz channel conditions. Section 4.5 presents the simulation results that validate the theoretical models and compare hybrid configurations against standalone systems. Lastly, Section 4.6 concludes the chapter with key insights and outlines future research directions, particularly focusing on adaptive control of IRS parameters and joint VLC-THz resource allocation for next-generation indoor networks.

4.3 System Model

4.3.1 IRS-aided THz Channel Model

The cascaded channel for the THz link with respect to the kth reflecting element of the IRS is modeled as $h_k = h_{1k}h_{2k}$, where h_{1k} and h_{2k} are the fading coefficients from the source to the IRS and from the IRS to the destination, respectively. The total fading coefficient is

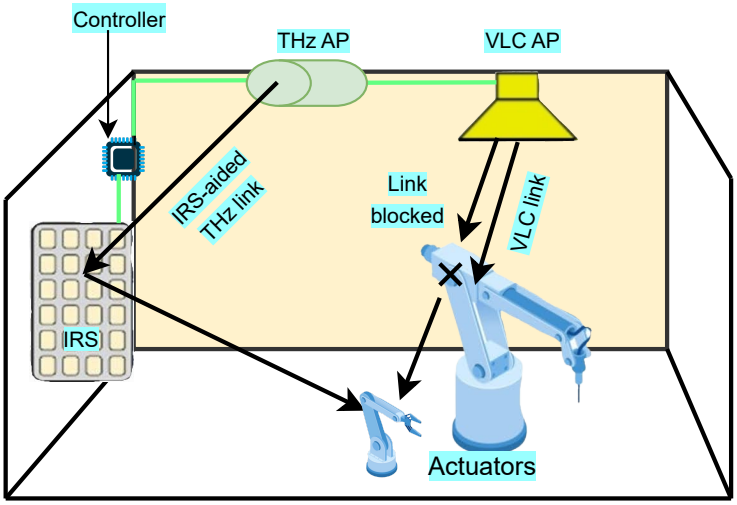

Figure 4.1: Hybrid VLC/IRS-aided THz system model

decomposed as

$$h_{jk} = h_{s_{jk}} h_{L_{jk}} h_{p_{jk}} \tag{4.1}$$

where $j = 1,2$, $h_{s_{jk}}$ is the small-scale fading component, $h_{p_{jk}}$ accounts for pointing errors, and $h_{L_{jk}} = h_a h_f$ represents the path gain. The term h_f is obtained using the Friis transmission equation, which is given by

$$h_f = \frac{c_s \sqrt{G_T}\sqrt{G_R}}{4\pi f_T d_T} \tag{4.2}$$

where G_T and G_R are the antenna gains, f_T is the operating THz frequency, c_s is the speed of light, and d_T is the link distance. The molecular absorption coefficient h_a is modeled as

$$h_a = \exp\left(-\frac{1}{2}\kappa_a(f_T) d_T\right) \tag{4.3}$$

where $\kappa_a(f_T)$ is the frequency-dependent absorption coefficient that quantifies molecular attenuation. The small-scale fading $h_{s_{jk}}$ follows an α–μ distribution and is given by

$$f_{h_{s_{jk}}}(h_s) = \frac{\alpha_{T_{jk}} \mu_{jk}^{\mu_{jk}} h_s^{\alpha_{T_{jk}}\mu_{jk}-1}}{\hat{h_T}^{\alpha_{T_{jk}}\mu_{jk}} \Gamma(\mu_{jk})} \exp\left(-\frac{\mu_{jk} h_s^{\alpha_{T_{jk}}}}{\hat{h_T}^{\alpha_{T_{jk}}}}\right) \tag{4.4}$$

The pointing error component $h_{p_{jk}}$ is uniformly distributed over $[0, S_0]$, where S_0 is the collected-power fraction. Now the PDF of pointing error component is given by

$$f_{h_{p_{jk}}}(h_p) = \frac{\zeta_{T_{jk}}^2}{S_0^{\zeta_{T_{jk}}^2}} h_p^{\zeta_{T_{jk}}^2 - 1}, \quad 0 \le h_p \le S_0 \tag{4.5}$$

where $\zeta_{T_{jk}} = V_{eq}/(2\sigma_T)$ is the pointing error coefficient, with σ_T denoting the jitter standard deviation, and V_{eq}, the equivalent beam waist, given by

$$V_{eq}^2 = \frac{v_d^2\sqrt{\pi}\,\mathrm{erf}(u_T)}{2u_T\exp(-u_T^2)} \tag{4.6}$$

PDF of the Elementary Sub-Link Gain

Using the Mellin–transform approach and substituting the PDFs above, the PDF of the composite sub-link envelope h_{jk} can be expressed in closed form as a Fox's H-function[1]

$$f_{h_{jk}}(h) = \frac{D_{jk}}{\alpha_{T_{jk}} E_{jk}^{(\zeta_{T_{jk}}^2-1)/2}}\, H_{1,2}^{2,0}\left(E_{jk}^{1/\alpha_{T_{jk}}} h \;\middle|\; \begin{matrix} \left(1+\frac{\zeta_{T_{jk}}^2-1}{\alpha_{T_{jk}}}, \frac{1}{\alpha_{T_{jk}}}\right) \\ \left(\frac{\zeta_{T_{jk}}^2-1}{\alpha_{T_{jk}}}, \frac{1}{\alpha_{T_{jk}}}\right), \left(\frac{\alpha_{T_{jk}}\mu_{jk}-1}{\alpha_{T_{jk}}}, \frac{1}{\alpha_{T_{jk}}}\right) \end{matrix} \right), \tag{4.7}$$

with

$$D_{jk} = \frac{\zeta_{T_{jk}}^2\, \mu_{jk}^{\zeta_{T_{jk}}^2/\alpha_{T_{jk}}}}{\hat{h}_T^{\alpha_{T_{jk}}}\Gamma(\mu_{jk}) S_0^{\zeta_{T_{jk}}^2}} \quad \text{and} \quad E_{jk} = \frac{\mu_{jk}}{(S_0\hat{h}_T)^{\alpha_{T_{jk}}}}.$$

End-to-End Cascaded Channel

Because $h_k = h_{1k}h_{2k}$, the end-to-end PDF can be obtained by Mellin convolution and is again expressible in Fox's H-function form [51]

$$\mathrm{f}_{h_k}(y) = D_{3k} H_{2,4}^{4,0}\left(E_{1k}^{1/\alpha_{T_{1k}}} E_{2k}^{1/\alpha_{T_{2k}}} y \;\middle|\; \begin{matrix} (\upsilon_{1k}^{(s)}, \Upsilon_{1k}^{(s)})_{s=1:2} \\ (\upsilon_{2k}^{(s)}, \Upsilon_{2k}^{(s)})_{s=1:4} \end{matrix} \right),$$

where the constants D_{3k}, $\upsilon_{ik}^{(\cdot)}$, and $\Upsilon_{ik}^{(\cdot)}$ follow directly from the parameter sets of the two sub-links.

Now, for calculating the PDF of complete IRS-assisted THz channel with N_T reflecting elements, i.e. $H = \sum_{k=1}^{N_T} h_k$, the MGF-based approach can be used. Firstly, the MGF of h_k is obtained by evaluating the Laplace integral of its PDF and simplifying using properties of Fox's H-function provided in [54]. This results in

$$\mathscr{M}_{h_k}(s) = D_{3k} H_{3,4}^{4,1}\left(E_{1k}^{\frac{1}{\alpha_{T_{1k}}}} E_{2k}^{\frac{1}{\alpha_{T_{2k}}}} s^{-1} \;\middle|\; \begin{matrix} (1,1), (\upsilon_{3k}^{(s)}, \Upsilon_{3k}^{(s)})_{s=1:2} \\ (\upsilon_{4k}^{(s)}, \Upsilon_{4k}^{(s)})_{s=1:4} \end{matrix} \right). \tag{4.8}$$

[1]The Fox's H-function form is obtained via [54, Eq. 07.34.26.0008.01].

The derived MGF can be utilized to deduce the PDF and CDF statistics for the complete THz channel. Applying Mellin's transformation and inverse Laplace transform, we obtain the final PDF and CDF, respectively as

$$f_H(h) = h^{-1} \prod_{d=1}^{N_T} D_{3d} H_{4,1:\ldots:3,4}^{0,0:0,1} \left(\begin{array}{c|c} hE_{11}^{\frac{1}{\alpha_{T_{11}}}} E_{21}^{\frac{1}{\alpha_{T_{21}}}} & -; \left\{(1,1), (\upsilon_{3k}^{(s)}, \Upsilon_{3k}^{(s)})_{s=1:2}\right\}_{k=1}^{N_T}; \\ \vdots & \\ hE_{1N_T}^{\frac{1}{\alpha_{T_{1N_T}}}} E_{2N_T}^{\frac{1}{\alpha_{T_{2N_T}}}} & \left(1; \{1\}_1^{N_T}\right); \left\{(\upsilon_{4k}^{(s)}, \Upsilon_{4k}^{(s)})_{s=1:4}\right\}_{k=1}^{N_T} \end{array} \right) \tag{4.9}$$

$$F_H(h) = \prod_{d=1}^{N_T} D_{3d} H_{4,1:\ldots:3,4}^{0,0:0,1} \left(\begin{array}{c|c} hE_{11}^{\frac{1}{\alpha_{T_{11}}}} E_{21}^{\frac{1}{\alpha_{T_{21}}}} & -; \left\{(1,1), (\upsilon_{3k}^{(s)}, \Upsilon_{3k}^{(s)})_{s=1:2}\right\}_{k=1}^{N_T}; \\ \vdots & \\ hE_{1N_T}^{\frac{1}{\alpha_{T_{1N_T}}}} E_{2N_T}^{\frac{1}{\alpha_{T_{2N_T}}}} & \left(0; \{1\}_1^{N_T}\right); \left\{(\upsilon_{4k}^{(s)}, \Upsilon_{4k}^{(s)})_{s=1:4}\right\}_{k=1}^{N_T} \end{array} \right) \tag{4.10}$$

Overall Instantaneous SNR Distribution

The overall instantaneous SNR for the RIS-assisted THz link is expressed as

$$\gamma_T = H^2 \Gamma_T, \tag{4.11}$$

where Γ_T denotes the average SNR of the THz link and $H = \sum_{k=1}^{N_T} h_k$ represents the equivalent channel gain incorporating the effects of generalized $\alpha-\mu$ fading, deterministic path loss, and pointing errors. By applying a power transformation on the random variable H, the PDF and CDF of γ_T are, respectively, given by

$$f_{\gamma_T}(\gamma) = \left(\frac{1}{2\sqrt{\gamma \Gamma_T}}\right) f_H\left(\sqrt{\frac{\gamma}{\Gamma_T}}\right), \tag{4.12}$$

$$F_{\gamma_T}(\gamma) = F_H\left(\sqrt{\frac{\gamma}{\Gamma_T}}\right). \tag{4.13}$$

Substituting the expression of $F_H(\cdot)$ based on the Fox's H-function representation of the underlying distribution, the final closed-form expression for the CDF of the RIS-assisted THz SNR with N_T IRS elements is given by

$$F_{\gamma_T}(\gamma) = \prod_{d=1}^{N_T} D_{3d}\, H_{4,1:\ldots:3,4}^{0,0:0,1} \left(\begin{array}{c|c} \sqrt{\frac{\gamma}{\Gamma_T}} E_{11}^{\frac{1}{\alpha_{T_{11}}}} E_{21}^{\frac{1}{\alpha_{T_{21}}}} & -; \left\{(1,1), \left(\upsilon_{3k}^{(s)}, \Upsilon_{3k}^{(s)}\right)_{s=1:2}\right\}_{k=1}^{N_T}; \\ \vdots & \\ \sqrt{\frac{\gamma}{\Gamma_T}} E_{1N_T}^{\frac{1}{\alpha_{T_{1N_T}}}} E_{2N_T}^{\frac{1}{\alpha_{T_{2N_T}}}} & \left(0; \{1\}_1^{N_T}\right); \left\{\left(\upsilon_{4k}^{(s)}, \Upsilon_{4k}^{(s)}\right)_{s=1:4}\right\}_{k=1}^{N_T} \end{array} \right). \tag{4.14}$$

4.4 Performance Analysis

This section presents the outage and error performance analysis of the proposed hybrid VLC/IRS-aided THz system. Closed-form expressions are derived by exploiting the CDF of VLC channel in (2.9) and the CDF of IRS-aided THz channel in (4.14).

4.4.1 Outage Probability

Let γ_{th} be the SNR threshold that triggers link switching. An outage occurs only when both links experience SNR lower than γ_{th}; hence

$$P_{\text{out}} = F_{\gamma_v}(\gamma_{\text{th}})\, F_{\gamma_T}(\gamma_{\text{th}}), \tag{4.15}$$

where $F_{\gamma_v}(\cdot)$ is given in (2.9) and $F_{\gamma_T}(\cdot)$ is given in (4.14). Substituting both CDFs yields the final outage-probability expression, which is given by

$$P_{\text{out}} = \left(\mathscr{B} - \Upsilon\, \gamma_{\text{th}}^{-\frac{1}{m+3}}\right) \prod_{d=1}^{N_T} D_{3d}\, H_{4,1:\ldots:3,4}^{0,0:0,1}\Big(\mathbf{Z}(\gamma_{\text{th}})\Big|\Theta\Big), \tag{4.16}$$

where $\mathbf{Z}(\gamma_{\text{th}}) = \sqrt{\gamma_{\text{th}}/\Gamma_T}\left[E_{11}^{1/\alpha_{T_{11}}} E_{21}^{1/\alpha_{T_{21}}}, \ldots, E_{1N_T}^{1/\alpha_{T_{1N_T}}} E_{2N_T}^{1/\alpha_{T_{2N_T}}}\right]^{\top}$ and Θ collects the pole/parameter sets defined in (4.14). This compact Fox's H-function representation is directly amenable to numerical evaluation via standard Mellin–Barnes quadrature techniques [52].

4.4.2 Average BER

As discussed before, we adopt binary PSK for both VLC and THz links. Now, by utilizing the generic expression for SER, which is given by (3.14), the average BER can be expressed through the Gauss–Laguerre quadrature rule and is given by

$$\overline{P}_e = \frac{\mathscr{A}\sqrt{\mathscr{B}}}{2\sqrt{\pi}} \sum_{p=1}^{\eta_f} \omega_p\, F_{\gamma}(\phi_p), \tag{4.17}$$

where

$$\omega_p = \frac{\phi_p\, \Gamma(p+0.5)}{p!\,(p+1)^2 \left(L_{p+1}^{-1/2}(\phi_p)\right)^2}, \qquad L_p^{-1/2}(x) = \sum_{i=0}^{p} \binom{p-\frac{1}{2}}{p-i} \frac{(-x)^i}{i!}. \tag{4.18}$$

The nodes ϕ_p are the roots of $L_{\eta_f}^{-1/2}(x)$ and η_f is the chosen Laguerre order.

Note that the average BER for VLC link is already derived in the Chapter 2. By substituting (4.14) in (4.19), the average BER of IRS-assisted THz system can be expressed as

$$\mathrm{BER}_t = \frac{\mathscr{A}\sqrt{\mathscr{B}}}{2\sqrt{\pi}} \sum_{p=1}^{\eta_f} \omega_p F_H\Big(\sqrt{\phi_p/\Gamma_T}\Big). \tag{4.19}$$

Now the final expression for average BER of hybrid VLC/IRS-assisted THz system is given by

$$\mathrm{BER}_{\mathrm{hybrid}} = \mathrm{BER}_v + F_{\gamma_v}(\gamma_{\mathrm{th}})\,\mathrm{BER}_t, \tag{4.20}$$

where $F_{\gamma_v}(\gamma_{\mathrm{th}})$ is given by (2.9). All the derived analytical expressions have been verified via Monte-Carlo simulations in the next section.

4.5 Results and Discussion

This section presents the simulation setup, empirical evaluation, and analytical verification of the proposed hybrid VLC/IRS-aided THz communication system. The system's performance is evaluated using both closed-form analytical expressions and Monte Carlo simulations to validate theoretical claims.The Fox's H-function in outage probability and average BER expressions are implemented using a Python code available in [55]. Unless otherwise stated, the parameters for the VLC system are adopted from Chapter 2, specifically Table 2.2, which defines the photodetector area, semi-angle at half power, and other optical channel parameters under the Lambertian radiation pattern. For the THz link, the generalized α–μ fading model is used to capture the channel behavior, with fading parameters set to $\alpha = \{2,4\}$ and $\mu = \{1,2\}$ in accordance with prior literature. These values allow us to study the impact of varying channel severity and path loss on system reliability. The threshold SNR for hard-switching between VLC and THz links is taken as 6 dB. The number of IRS elements are considered to be $N = 2$.

Fig. 4.2 illustrates the outage probability versus average SNR for the proposed hybrid VLC/IRS-aided THz system. The performance of three configurations is compared: standalone VLC link, hybrid VLC/THz system, and the proposed VLC/IRS-aided THz system. The standalone VLC system is configured with a photodetector area $A_p = 0.10\,\mathrm{cm}^2$, responsivity $R_p = 0.64\,\mathrm{A/W}$, and cell radius $r_{\max} = 2\,\mathrm{m}$. This setup results in a relatively high outage probability, remaining above 0.59 even at 20 dB SNR, highlighting its susceptibility to performance degradation under challenging conditions. The hybrid VLC/THz system is then evaluated with fading parameters $\mu = 1$ and $\alpha = 2$, showing significant performance gains. At 10 dB, the outage probability reduces to approximately 0.021, indicating a notable

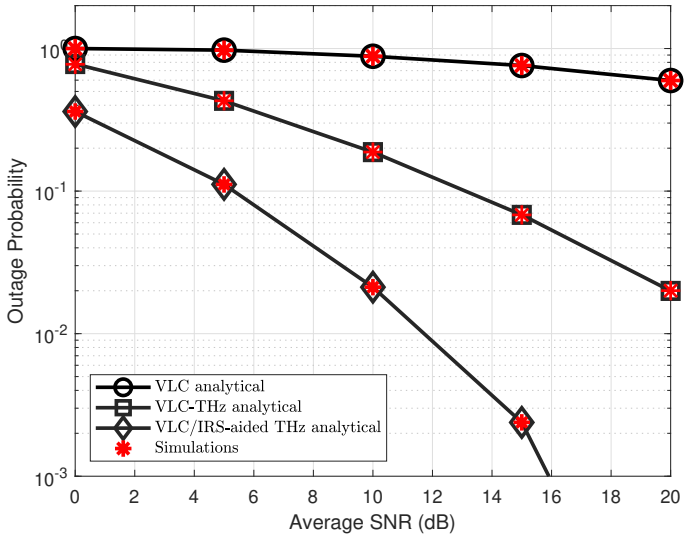

Figure 4.2: Outage probability of VLC and hybrid VLC/ IRS aided THz System

SNR gain of 10 dB compared to the VLC-only system at similar outage levels. Further performance improvement is observed in the proposed VLC/IRS-aided THz configuration, where the IRS is composed of $N = 2$ reflecting elements and uses the same fading parameters ($\mu = 1$, $\alpha = 2$). This configuration achieves an outage probability of 0.020 at 20 dB, showcasing enhanced link robustness due to IRS-induced beamforming gains. Compared to the non-IRS hybrid system, the IRS-aided version achieves the same outage at a lower SNR, implying additional link margin and SNR savings. These results confirm the effectiveness of integrating IRS into the hybrid VLC/THz architecture, which considerably improves outage performance in low-to-moderate SNR regimes.

Fig. 4.3 compares the average BER performance for four configurations: standalone VLC, hybrid VLC/THz with two different fading profiles, and hybrid VLC/IRS-aided THz.The VLC system is configured with $A_p = 0.10\,\text{cm}^2$, and it yields a BER of approximately 0.0346 at 20 dB. In contrast, the hybrid VLC/THz system with $\mu = 1$, $\alpha = 2$ achieves a better BER performance of approximately 0.01429 at 12 dB, indicating a substantial SNR gain of about 8 dB over the standalone VLC link. Further performance enhancement is observed with the hybrid VLC/THz system configured with stronger fading parameters ($\mu = 2$, $\alpha = 4$), which achieves a BER of 0.0106 at 20 dB, thus outperforming the previous configuration. Notably, the hybrid VLC/IRS-aided THz system with parameters $\mu = 2$, $\alpha = 4$, and $N = 2$ IRS elements achieves a BER of approximately 0.0282 at only 0 dB, which is equivalent to the BER of the VLC-only system at 20 dB. This translates to an approximate SNR gain

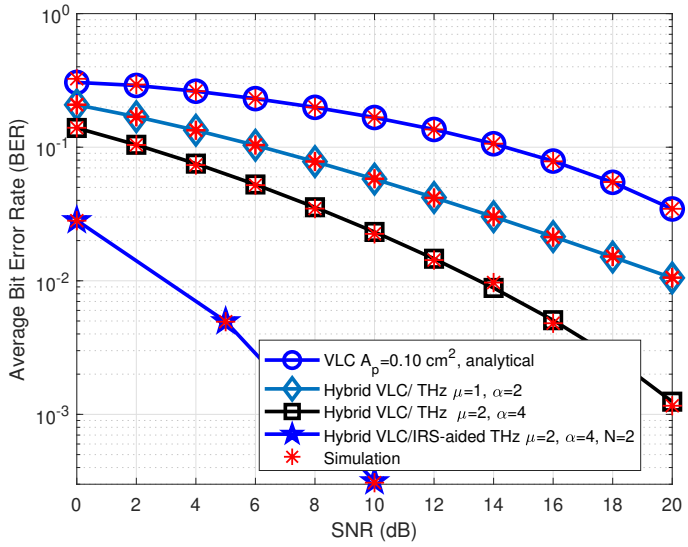

Figure 4.3: Average BER of VLC and hybrid VLC/ IRS aided THz System

of 20 dB, clearly highlighting the effectiveness of IRS integration in improving link quality and BER performance under harsh channel conditions.

4.6 Conclusion and Future Work

In this chapter, we proposed a hybrid VLC/IRS-aided THz communication system to overcome the limitations of standalone VLC and conventional THz systems in complex environments subject to blockages, severe path loss, and high sensitivity to pointing errors. The system implements a hard-switching mechanism in which the IRS-aided THz link serves as a backup whenever the instantaneous SNR of the VLC link drops below a predefined threshold. The VLC link follows Lambertian emission, while the THz channel gain is modeled by a cascaded product of generalized α-μ fading and pointing error distributions. Furthermore, the IRS-aided THz channel gain distribution was expressed using a tractable Fox's H-function framework to capture its statistical characteristics. Closed-form analytical expressions were derived for outage probability and average BER. The BER for the THz component was computed using Gauss–Laguerre quadrature due to the complexity of the fading model. All results were validated against Monte-Carlo simulations. Numerical analysis demonstrated significant SNR gains for the hybrid VLC/IRS-aided THz system over both standalone VLC and traditional hybrid VLC/THz systems. In particular, the integration of IRS elements showed measurable improvement in link reliability and BER performance

even under low SNR conditions, confirming the benefits of intelligent reflection in THz systems.

Future research will consider the use of dynamic IRS phase adjustment to optimize end-to-end THz gain in real time. Machine learning techniques will be explored to enhance link switching and IRS element control based on real-time channel estimates. Extensions of this work include multi-IRS and multi-user configurations, as well as the incorporation of joint VLC/IRS beam alignment strategies. Additional investigation will focus on adaptive modulation, energy-efficient designs, and seamless integration with existing RF/VLC infrastructures to support emerging 6G applications in smart indoor and aerial communication networks.

Chapter 5

Conclusions and Future Works

This thesis investigated and analyzed three advanced hybrid optical–wireless communication architectures that leverage IRS, THz, and VLC technologies to overcome the limitations of standalone VLC systems in complex environments. The key objective was to develop robust hybrid models capable of maintaining link reliability, reducing outage probability, and improving BER performance under challenging propagation conditions.

Overall Conclusion

In the first phase of the thesis, an IRS-aided hybrid RF/VLC communication system was proposed to improve indoor communication performance, especially under non-LoS and obstruction scenarios. Closed-form expressions for outage probability, average BER, and outage capacity were derived, accounting for Lambertian VLC modeling and Nakagami-m fading for the RF channel. Numerical simulations validated the theoretical derivations and demonstrated that integrating IRS with VLC/RF significantly enhances reliability and signal quality.

Next, a hybrid VLC/THz system was introduced to address the bandwidth limitations and short-range constraints of VLC in dynamic environments. Here, the THz link was modeled using an α-μ fading distribution, and analytical expressions for outage probability, average BER, and outage capacity were derived. Gauss–Laguerre quadrature was used to compute BER under complex channel fading conditions. Simulation results revealed notable SNR improvements of the hybrid VLC/THz system over standalone VLC links, especially in scenarios affected by path loss and blockage.

Finally, the thesis proposed a more advanced hybrid VLC/IRS-aided THz communication system. In this model, the THz link benefits from IRS-based beam steering and power focusing. The end-to-end IRS-assisted THz channel was modeled using generalized α-μ fading, pointing error distribution, and Fox–H function representations. Closed-form expressions were derived for outage probability and BER. This system outperformed both standalone and conventional hybrid configurations, with simulations confirming significant SNR gains and BER improvements at low SNR regimes, attributed to intelligent control of the reflected THz waves.

Future Research Directions

Building upon the insights from this work, the following future research directions are proposed:

- **Machine Learning for Intelligent Link Switching:** Adaptive switching between VLC, RF, and THz links based on real-time SNR and environmental context can be optimized using reinforcement learning or deep learning algorithms.
- **Dynamic IRS Configuration:** Further exploration of real-time IRS phase shift optimization and beamforming, specifically tailored for THz bands, can enhance end-to-end gain and support mobility scenarios.
- **Joint VLC/THz/IRS System Design:** Future studies can focus on the design of fully integrated tri-band hybrid systems that combine VLC, THz, and RF with coordinated IRS control for seamless transitions and multi-user support.
- **Mobility and CSI Acquisition:** Practical challenges such as user mobility, Doppler effects, and channel estimation for high-frequency links must be addressed through novel mobility modeling and channel state information (CSI) feedback mechanisms.
- **Multi-hop and Multi-IRS Topologies:** Expansion to multi-hop relay-assisted systems and networks with multiple IRS panels can provide extended coverage and higher reliability in large indoor or smart factory environments.
- **Resource Allocation and Energy Efficiency:** Future systems should incorporate joint power allocation, modulation adaptation, and energy-efficient protocol design

to align with the low-latency, high-throughput requirements of 6G networks.

Overall, the outcomes of this thesis demonstrate the viability and benefits of hybrid VLC/IRS-aided RF/THz communication architectures and provide a strong foundation for future research in the domain of intelligent optical–wireless communications.

Publications from Thesis

- K. Tripathi and S. R., "Outage Analysis of Hybrid VLC/Multi-IRS-aided RF Communication System," in *Proc. 2025 17th International Conference on Communication Systems and Networks (COMSNETS),* Bengaluru, India, 2025, pp. 931–935.

- K. Tripathi. P. Sharma, and Swaminathan R, "System-level analysis of hybrid VLC/IRS-enhanced RF communication," ***Optical and Quantum Electronics (Springer)***, vol. 57, no. 398, pp. 1-27, June 2025, DOI: 10.1007/s11082-025-08338-2, Published

- K. Tripathi, P. Sharma, and R. Swaminathan, "Performance analysis of hybrid VLC/IRS-Aided THz communication system," *Springer Photonic Network Communications*, **(Manuscript Under Preparation)**.

Appendix

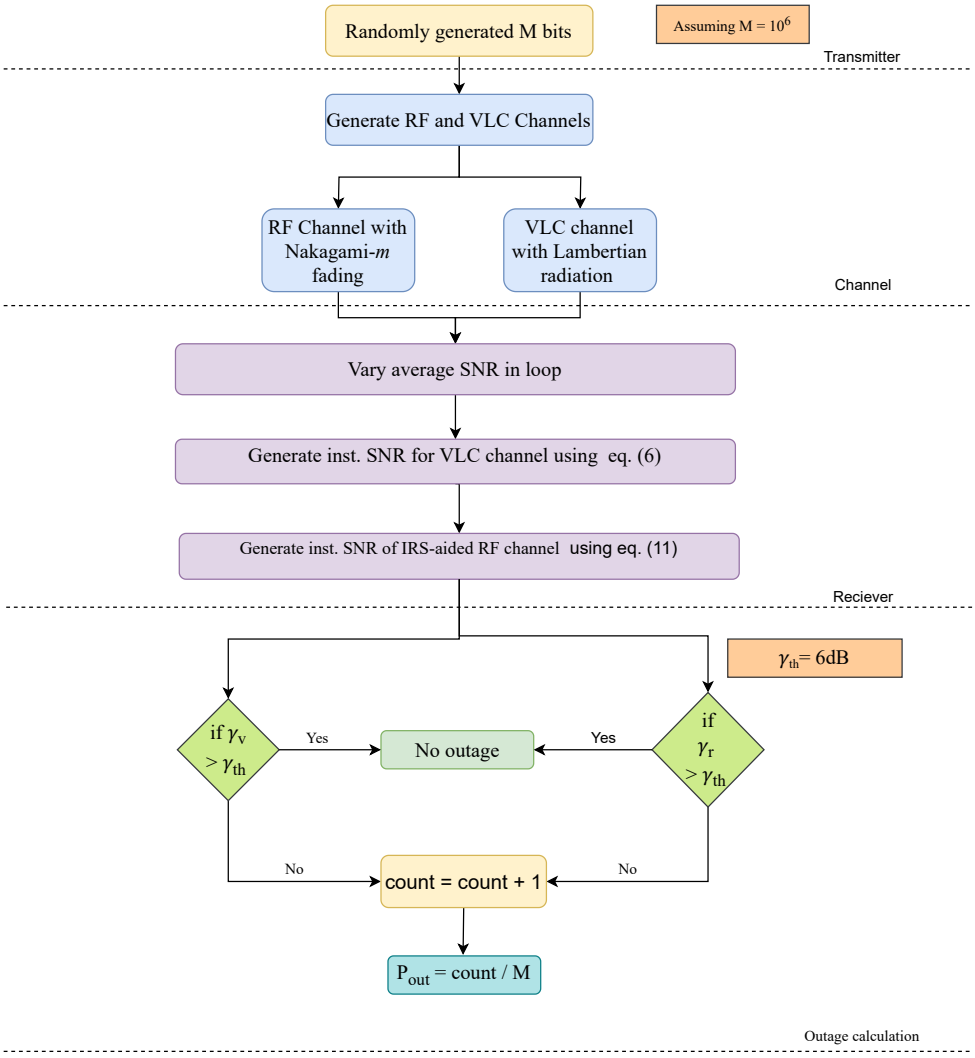

Figure 5.1: Flowchart for computing outage probability using Monte-Carlo simulations.

The detailed Monte-Carlo simulation flowchart for calculation of the outage probability of the proposed hybrid system is shown in Fig. 5.1. This is achieved by transmitting $M = 10^6$ bits over the hybrid VLC and IRS-assisted RF channels and calculating

the outage based on the instantaneous SNR values of both systems when they fall below the threshold.

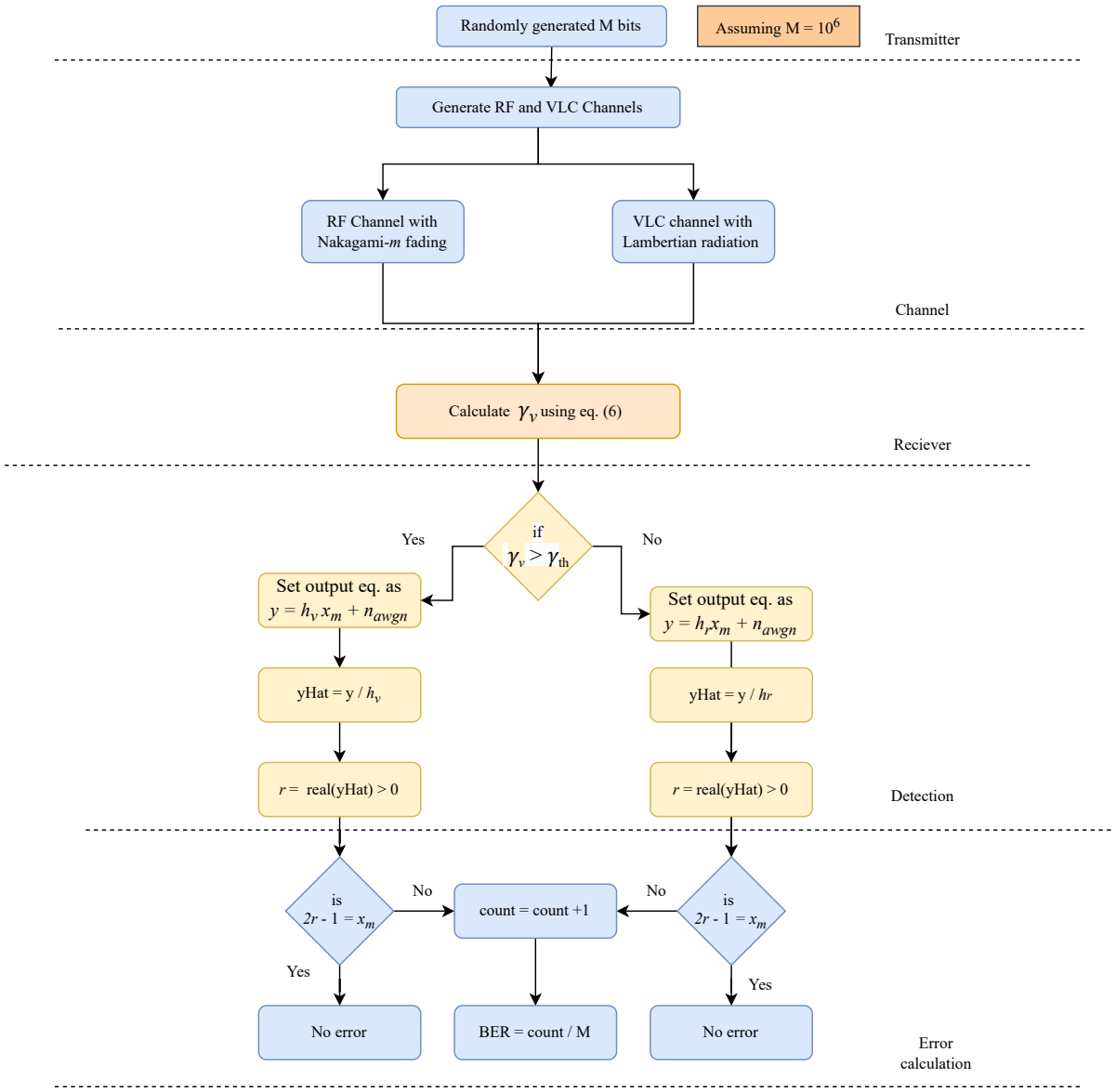

Figure 5.2: Flowchart for computing average BER using Monte-Carlo simulations.

Similarly in Fig. 5.2, the detailed Monte-Carlo simulation flowchart is presented for calculation of average BER of the proposed hybrid system. Here the channel coefficients are generated and the generated input symbols are transmitted over the VLC or IRS-assisted RF channel depending upon the instantaneous SNR values. The received signals over the VLC and RF channels are, respectively, given by

$$y = h_v x_m + n_{awgn} \quad \text{and} \quad y = h_r x_m + n_{awgn}, \tag{5.1}$$

where h_v is the channel gain coefficient for the VLC link, h_r is the channel gain coefficient for the IRS-assisted RF link, x_m represents the transmitted BPSK symbol, and n_{awgn} denotes the additive white Gaussian noise (AWGN) with zero mean and variance σ^2. After equalization, the detected BPSK symbols are compared with the transmitted symbols to calculate the average BER.

Bibliography

[1] A. Memedi and F. Dressler. “Vehicular visible light communications: a survey”. In: *IEEE Commun. Surv. Tutor.* **23**.1 (2021), pp. 161–181. DOI: 10.1109/COMST.2020.3034224.

[2] A. Jovicic, J. Li, and T. Richardson. “Visible light communication: opportunities, challenges and the path to market”. In: *IEEE Commun. Mag.* **51**.12 (2013), pp. 26–32. DOI: 10.1109/MCOM.2013.6685754.

[3] L.E.M. Matheus et al. “Visible light communication: concepts, applications and challenges”. In: *IEEE Commun. Surv. Tutor.* **21**.4 (2019), pp. 3204–3237. DOI: 10.1109/COMST.2019.2913348.

[4] N. An et al. “IRS-assisted aggregated VLC-RF system: resource allocation for energy efficiency maximization”. In: *IEEE Wirel. Commun.* **23**.10 (2024), pp. 12578–12593. DOI: 10.1109/COMST.2019.2913348.

[5] X. Wu et al. “Hybrid LiFi and WiFi networks: a survey”. In: *IEEE Commun. Surv. Tutor.* **23**.2 (2021), pp. 1398–1420. DOI: 10.1109/COMST.2021.3058296.

[6] G. Pan et al. “Secure cooperative hybrid VLC-RF systems”. In: *IEEE Wirel. Commun.* **19**.11 (2020), pp. 7097–7107. DOI: 10.1109/TWC.2020.3007937.

[7] I. F. Akyildiz, J. M. Jornet, and C. Han. “Terahertz band: Next frontier for wireless communications”. In: *Phys. Commun.* **12** (2014). Sep., pp. 16–32.

[8] A.-A. A. Boulogeorgos et al. “Wireless terahertz system architectures for networks beyond 5G”. In: *Terranova Consortium, White Paper 1.0* (2018). Jul.

[9] N. Choudhary, S. Joshi, and V.K. Chaubey. “Outage analysis of an IRS-assisted 5G and beyond wireless communications system”. In: *2023 IEEE 97th Vehicular Tech-*

nology Conference (VTC2023-Spring). Florence, Italy, 2023, pp. 1–5. DOI: 10.1109/VTC2023-Spring57618.2023.10199744.

[10] A.M. Tota Khel and K.A. Hamdi. "Performance analysis of IRS-assisted full-duplex wireless communication systems with interference". In: *IEEE Commun. Lett.* **26**.9 (2022), pp. 2027–2031. DOI: 10.1109/LCOMM.2022.3187677.

[11] N. Qarinah et al. "Performance evaluation of CRC-16 in indoor visible light communication (VLC) against jamming attack". In: *2023 IEEE Asia Pacific Conference on Wireless and Mobile (APWiMob)*. Bali, Indonesia, 2023, pp. 237–242. DOI: 10.1109/APWiMob59963.2023.10365651.

[12] A.R. Ndjiongue and K. Ouahada. "Capacity of outdoor VLC links using a visible LASER beam". In: *2019 International Symposium on Networks, Computers and Communications (ISNCC)*. Istanbul, Turkey, 2019, pp. 1–6. DOI: 10.1109/ISNCC.2019.8909107.

[13] Y. Wang et al. "Enhanced performance of a high-speed WDM CAP64 VLC system employing Volterra series-based nonlinear equalizer". In: *IEEE Photonics J.* **7**.3 (2015), pp. 1–7. DOI: 10.1109/JPHOT.2015.2436911.

[14] S. Ullah, S.U. Rehman, and P.H.J. Chong. "Performance analysis of defused VLC channel for mobile environment". In: *2019 29th International Telecommunication Networks and Applications Conference (ITNAC)*. Auckland, New Zealand, 2019, pp. 1–6. DOI: 10.1109/ITNAC46935.2019.9078022.

[15] R.N. Sathisha, F. Ahmed, and V. Raghunathan. "Demonstration of RF-VLC handover using receiver side channel selection". In: *Proc. IEEE COMSNETS*. Bangalore, India, 2023, pp. 382–386. DOI: 10.1109/COMSNETS56262.2023.10041361.

[16] E. Basar et al. "Wireless communications through reconfigurable intelligent surfaces". In: *IEEE Access* **7** (2019), pp. 116753–116773. DOI: 10.1109/ACCESS.2019.2935192.

[17] S. Mondal et al. "Outage probability analysis of hard-switching based mixed FSO/IRS-aided RF communication". In: *2023 National Conference on Communications (NCC)*. Guwahati, India, 2023, pp. 1–6. DOI: 10.1109/NCC56989.2023.10067918.

[18] C. Han and Y. Chen. "Propagation modeling for wireless communications in the terahertz band". In: *IEEE Commun. Mag.* **56**.6 (2018). Jun., pp. 96–101.

[19] G. A. Siles, J. M. Riera, and P. García-del-Pino. “Atmospheric attenuation in wireless communication systems at millimeter and THz frequencies”. In: *IEEE Antennas Propag. Mag.* **57**.1 (2015). Feb., pp. 48–61.

[20] J. Kokkoniemi, J. Lehtomäki, and M. Juntti. “Simplified molecular absorption loss model for 275–400 gigahertz frequency band”. In: *Proc. 12th Eur. Conf. Antennas Propag. (EuCAP)* (2018). London, U.K., Apr., pp. 1–5.

[21] C. Han, A. O. Bicen, and I. F. Akyildiz. “Multi-ray channel modeling and wideband characterization for wireless communications in the terahertz band”. In: *IEEE Trans. Wireless Commun.* **14**.5 (2015). May, pp. 2402–2412.

[22] J. M. Jornet and I. F. Akyildiz. “Channel modeling and capacity analysis for electromagnetic wireless nanonetworks in the terahertz band”. In: *IEEE Trans. Wireless Commun.* **10**.10 (2011). Oct., pp. 3211–3221.

[23] K. Yang et al. “Numerical analysis and characterization of THz propagation channel for body-centric nano-communications”. In: *IEEE Trans. THz Sci. Technol.* **5**.3 (2015). May, pp. 419–426.

[24] A. Afsharinejad et al. “An initial path-loss model within vegetation in the THz band”. In: *Proc. 9th Eur. Conf. Antennas Propag. (EuCAP)* (2015). Lisbon, Portugal, May, pp. 1–5.

[25] H. Elayan et al. “Terahertz channel model and link budget analysis for intrabody nanoscale communication”. In: *IEEE Trans. Nanobiosci.* **16**.6 (2017). Sep., pp. 491–503.

[26] S. Kim and A. Zajić. “Statistical modeling of THz scatter channels”. In: *Proc. 9th Eur. Conf. Antennas Propag. (EuCAP)* (2015). Lisbon, Portugal, May, pp. 1–5.

[27] S. Kim and A. Zajić. “Statistical modeling and simulation of short-range device-to-device communication channels at sub-THz frequencies”. In: *IEEE Trans. Wireless Commun.* **15**.9 (2016). Sep., pp. 6423–6433.

[28] J. Kokkoniemi, J. Lehtomäki, and M. Juntti. “Frequency domain scattering loss in THz band”. In: *Proc. Global Symp. Millim.-Waves (GSMM)* (2015). Montreal, QC, Canada, May, pp. 1–3.

[29] A. R. Ekti et al. “Statistical modeling of propagation channels for terahertz band”. In: *Proc. IEEE Conf. Standards Commun. Netw. (CSCN)* (2017). Helsinki, Finland, Sep., pp. 275–280.

[30] S. Priebe, M. Jacob, and T. Kürner. “The impact of antenna directivities on THz indoor channel characteristics”. In: *Proc. 6th Eur. Conf. Antennas Propag. (EuCAP)* (2012). Prague, Czech Republic, Mar., pp. 478–482.

[31] A. Afsharinejad et al. “A path-loss model incorporating shadowing for THz band propagation in vegetation”. In: *Proc. Global Commun. Conf. (GLOBECOM)* (2015). San Diego, CA, USA, Dec., pp. 1–6.

[32] C. Han and I. F. Akyildiz. “Three-dimensional end-to-end modeling and analysis for graphene-enabled terahertz band communications”. In: *IEEE Trans. Veh. Technol.* **66**.7 (2017). Jul., pp. 5626–5634.

[33] C. Liu et al. “Average capacity for heterodyne FSO communication systems over gamma-gamma turbulence channels with pointing errors”. In: *Electron. Lett.* **46**.12 (2010). Jun., pp. 851–853.

[34] S. Koenig et al. “Wireless sub-THz communication system with high data rate”. In: *Nature Photon.* **7** (2013). Oct., p. 977.

[35] I. Kallfass et al. “Towards MMIC-based 300 GHz indoor wireless communication systems”. In: *IEICE Trans. Electron.* **98**.12 (2015). Dec., pp. 1081–1090.

[36] T. Schenk. “RF Imperfections in High-rate Wireless Systems: Impact and Digital Compensation”. In: *Springer* (2008). Dordrecht, The Netherlands.

[37] A.-A. A. Boulogeorgos et al. “I/Q-imbalance self-interference coordination”. In: *IEEE Trans. Wireless Commun.* **15**.6 (2016). Jun., pp. 4157–4170.

[38] M. Elkhouly et al. “A 240 GHz direct conversion IQ receiver in 0.13 µm SiGe BiCMOS technology”. In: *Proc. IEEE Radio Freq. Integr. Circuits Symp. (RFIC)* (2013). Seattle, WA, USA, Jun., pp. 305–308.

[39] A. A. Abidi. “Direct-conversion radio transceivers for digital communications”. In: *IEEE J. Solid-State Circuits* **30**.12 (1995). Dec., pp. 1399–1410.

[40] B.A. Vijayalakshmi et al. “VLC system using LEDs for transmitting underwater information”. In: *J. Opt.* **53** (2024).

[41] H. Sharma and R.K. Jha. “VLC Enabled Hybrid Wireless Network for B5G/6G Communications”. In: *Wirel. Pers. Commun.* **124**.2 (2022), pp. 1741–1771. DOI: 10.1007/s11277-021-09429-5.

[42] H. Haas. “Visible light communication”. In: *2015 Optical Fiber Communications Conference and Exhibition (OFC)*. Los Angeles, CA, USA, 2015, pp. 1–72.

[43] L. Yin, X. Wu, and H. Haas. “On the performance of non-orthogonal multiple access in visible light communication”. In: *2015 IEEE 26th Annual International Symposium on Personal, Indoor, and Mobile Radio Communications (PIMRC)*. Hong Kong, China, 2015, pp. 1354–1359.

[44] R. Swaminathan and R. Roy. “HSSEC strategy for decode-and-forward-relaying systems over Nakagami-m fading channels”. In: *IET Commun.* **10**.18 (2016), pp. 2621–2635.

[45] I. S. Gradshteyn and I. M. Ryzhik. *Tables of Integrals, Series, and Products*. 7th ed. Amsterdam, The Netherlands: Academic Press, 2007.

[46] Deepshikha Singh, R. Swaminathan, and Anh T. Pham. “Multiple HAPS-based space-air-ground network with FSO communication: A performance analysis”. In: *Applied Optics* **63**.9 (2024), pp. 2362–2375.

[47] Anshul Vats, Mona Aggarwal, and Swaran Ahuja. “Outage and Error Analysis of Three-Hop Hybrid VLC/FSO/VLC-Based Relayed Optical Wireless Communication System”. In: *Emerging Telecommunications Technologies* **30**.50 (2019), e3544.

[48] J. Liu, L. Ma, and Z. He. “Underwater Visible Light Mobile Communication Using a Gain Feedback Control Method With Dynamic Threshold”. In: *IEEE Photonics Journal* **15**.6 (Dec. 2023), pp. 1–6. DOI: 10.1109/JPHOT.2023.3333227.

[49] A.-A. A. Boulogeorgos et al. “Terahertz technologies to deliver optical network quality of experience in wireless systems beyond 5G”. In: *IEEE Commun. Mag.* **56**.6 (2018). Jun., pp. 144–151.

[50] A. S. Cacciapuoti et al. “Beyond 5G: THz-based medium access protocol for mobile heterogeneous networks”. In: *IEEE Commun. Mag.* **56**.6 (2018). Jun., pp. 110–115.

[51] A.-A. A. Boulogeorgos et al. “Performance evaluation of THz wireless systems operating in 275–400 GHz band”. In: *Proc. IEEE Veh. Technol. Conf. (VTC)* (2018). Jun., pp. 1–5.

[52] A.-A. A. Boulogeorgos, E. N. Papasotiriou, and A. Alexiou. “Analytical performance assessment of THz wireless systems”. In: *IEEE Access* 7 (2019), pp. 11436–11453.

[53] P. Concus et al. “Tables for the evaluation of $\int_0^\infty x^\beta e^{-x} f(x)\,dx$ by Gauss–Laguerre quadrature”. In: *Math. Comput.* **17**.83 (1963), pp. 245–256.

[54] A. M. Mathai, R. Saxena, and H. Haubold. *The H-Function: Theory and Applications*. New York, NY, USA: Springer, 2010.

[55] H. R. Alhennawi et al. “Closed-form exact and asymptotic expressions for the symbol error rate and capacity of the H-function fading channel”. In: *IEEE Transactions on Vehicular Technology* 65.4 (Apr. 2016), pp. 1957–1974.